OCT 31 1949 REC'D

CLASSIFICATION CANCELLED

Copy 1

RM SA9J14

NACA RM SA9J14

PERMANENT FILE COPY

[redacted]

Source of Acquisition
CASI Acquired

NACA

RESEARCH MEMORANDUM

for the

CLASSIFICATION CANCELLED

Bureau of Aeronautics, Navy Department

THE EFFECTS OF HORIZONTAL TAIL LOCATION AND WING MODIFICATIONS ON THE HIGH-SPEED STABILITY AND CONTROL CHARACTERISTICS OF A 0.17-SCALE MODEL OF THE McDONNELL XF2H-1 AIRPLANE (TED No. NACA DE336)

By Horace F. Emerson and John A. Axelson

Ames Aeronautical Laboratory
Moffett Field, Calif.

[redacted]

CLASSIFICATION CANCELLED

J. W. Crowley 3/11/55

NACA change 2959

OES

Status: INACTIVE

EDITING WAIVED

NATIONAL ADVISORY COMMITTEE FOR AERONAUTICS

WASHINGTON

October 14, 1949

CLASSIFICATION CANCELLED

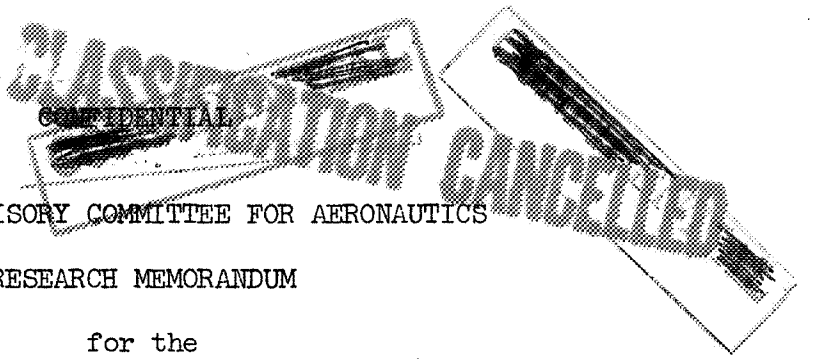

NATIONAL ADVISORY COMMITTEE FOR AERONAUTICS

RESEARCH MEMORANDUM

for the

Bureau of Aeronautics, Navy Department

THE EFFECTS OF HORIZONTAL-TAIL LOCATION AND WING MODIFICATIONS ON THE HIGH-SPEED STABILITY AND CONTROL CHARACTERISTICS OF A 0.17-SCALE MODEL OF THE McDONNELL XF2H-1 AIRPLANE (TED No. NACA DE336)

By Horace F. Emerson and John A. Axelson

SUMMARY

An additional series of high-speed wind-tunnel tests of a modified 0.17-scale model of the McDonnell XF2H-1 airplane was conducted to evaluate the effects of a reduction in the thickness-to-chord ratios of the tail planes, the displacement of the horizontal tail relative to the vertical tail, and the extension of the trailing edge of the wing. Two tail-intersection fairings designed to improve the flow at the tail were also tested. The pitching-moment characteristics of the model were improved slightly by the use of the thinner tail sections. Rearward or rearward and downward displacements of the horizontal tail increased the critical Mach number at the tail intersection from 0.725 to a maximum of 0.80, but caused an excessive change in pitching-moment coefficient at the higher Mach numbers. Extending the trailing edge of the wing did not improve the static longitudinal-stability characteristics, but increased the pitching-down tendency between 0.725 and 0.825 Mach numbers prior to the pitching-up tendency. The extended wing did, however, increase the Mach numbers at which these tendencies occurred. The increase in the Mach numbers of divergence and the tuft studies indicate a probable increase in the buffet limit of the prototype airplane. No perceptible improvement of flow at the tail intersection was observed with the two fairings tested on the forward tail configuration.

INTRODUCTION

As a result of previous wind-tunnel tests of two versions of the 0.17-scale model of the McDonnell XF2H-1 airplane, the Bureau of Aeronautics, Navy Department, requested additional wind-tunnel tests of the model modified to comply with the recommendations made in reference 1.

This investigation evaluates the effect of a reduction in the thickness-to-chord ratio of the tail planes, the effect of displacing the horizontal-tail plane relative to the vertical-tail plane, and the effect of extending the trailing edge of the wing to reduce the trailing-edge

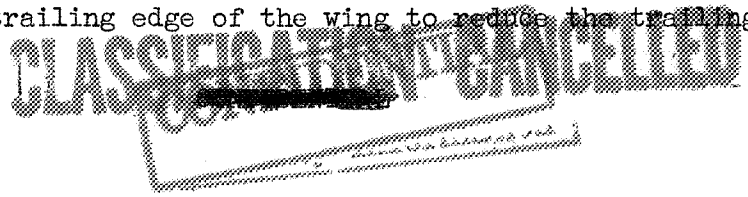

angle and the thickness-to-chord ratio of the wing. Data for two wing modifications, designated W_3 and W_4, tested on the model in combination with various tail assemblies, designated H_2, H_3, H_4, and H_5, are presented in this report.

The wind-tunnel tests were conducted through a Mach number range from 0.40 to 0.90, corresponding under the test conditions to a Reynolds number range from 3.2 to 5.1 million.

SYMBOLS

The coefficients and symbols are defined as follows:

C_D drag coefficient $\left(\frac{\text{drag}}{qS}\right)$

C_L lift coefficient $\left(\frac{\text{lift}}{qS}\right)$

C_h hinge-moment coefficient $\left(\frac{\text{hinge moment}}{2qM_A}\right)$

C_m pitching-moment coefficient about the airplane lateral axis through the quarter point of the mean aerodynamic chord $\left(\frac{\text{pitching moment}}{qS\bar{c}}\right)$

M Mach number

M_A moment about hinge line of control-surface area behind the hinge line, feet cubed

M_{cr} critical Mach number, corresponding to first occurrence of local sonic velocity

P pressure coefficient $\left[\frac{(\text{local static pressure})-(\text{free-stream static pressure})}{q}\right]$

P_{cr} critical pressure coefficient, corresponding to local sonic velocity

S wing area, square feet

V velocity, feet per second

b wing span, feet

c local chord, feet

$\bar{c}$ wing mean aerodynamic chord $\left(\frac{\int_0^{b/2} c^2 dy}{\int_0^{b/2} c\, dy}\right)$, feet

i	incidence, degrees
q	dynamic pressure $\left(\frac{1}{2}\rho V^2\right)$, pounds per square foot
$\frac{t}{c}$	thickness-to-chord ratio
y	lateral coordinate, measured from plane of symmetry, feet
α	angle of attack of fuselage reference line, degrees
δ	control-surface deflection, positive when trailing edge is lowered, degrees
ρ	free-stream mass density, slugs per cubic foot

Subscripts

e	elevator
t	horizontal tail
u	uncorrected

APPARATUS AND TESTS

Model Description and Support System

Figure 1 shows for comparison the plan forms of the two wings (W_3 and W_4) tested on the model with the revised wing (W_2) of reference 1. Figure 2 presents the geometric characteristics of wings W_3 and W_4, while figure 3 shows the relative locations of the horizontal-tail planes (H_2, H_3, H_4, and H_5) with respect to the vertical tail and gives in tabular form information on the tail assemblies. Photographs of the model with W_3H_3 and W_3H_5 are presented in figure 4. Dimensional data on wing W_2 and tail H_2, as well as a detailed description of the model and the support system, are given in reference 1.

In order to facilitate the comparison between the data obtained in this investigation and those presented in reference 1, the wing area of W_2 was used in reducing the data to coefficient form. The areas of W_3 and W_4 exceeded that of W_2 by approximately 8 and 12 percent, respectively. The fuselage was included in all tests, but for simplicity of notation the complete model is identified by the appropriate W and H designations of the wing and tail. Only the wing designation W is used to identify the model with the horizontal and vertical-tail assembly removed.

Lift, drag, and pitching moment were measured with each of the wings and with various tail configurations on the model. Wing W_3 was tested

without tail surfaces and with H_2, H_3, H_4, and H_5, while W_4 was tested without tail surfaces and with H_4. Elevator hinge moments were measured with H_2 and W_3 on the model, but without the horn balance of reference 1 on the elevator. Two tail-intersection fairings, called the bullet fairing and the hourglass fairing, were tested with the tail in position A (fig. 3) in an effort to improve the flow at the intersection without displacing the horizontal tail. Photographs of the two fairings are included in the report and will be introduced in the discussion of the tails.

Pressure distributions were measured on W_3 at wing station 17.41 and at the tail intersections of H_3, H_4, and H_5 to determine minimum-pressure locations and critical Mach numbers. No pressure distributions were measured with W_4 on the model.

PRESENTATION OF DATA

Corrections

The corrections applied to the data and the accuracy of the measured values are those given in reference 1.

Order of Presentation of Data

Basic tail-off force coefficients for both wings (W_3 and W_4) are presented in figures 5, 6, and 7. Tail-on drag polars, pitching-moment curves, and lift curves are shown in figures 8, 9, and 10, for each wing in combination with tail H_4. The lift and drag data for W_3 with the other tail configurations are not presented because they did not differ significantly from those obtained for W_3H_4. The variations of pitching-moment coefficient with lift coefficient for W_3H_2, W_3H_3, W_3H_4, and W_3H_5 at various elevator deflections are shown in figures 11, 12, 13, and 14.

Variations with Mach number of several aerodynamic characteristics are presented in figures 15 through 18 for comparing wings W_3 and W_4. Figures 19 and 20 present the variations of pitching-moment coefficient with Mach number for all the tail-on configurations investigated. Figure 21 compares the longitudinal-control characteristics of W_3H_3, W_3H_4, and W_3H_5. Figure 22 presents the variations with Mach number of the neutral point and the elevator-effectiveness parameter for several wing and tail combinations. Figure 23 shows elevator hinge-moment coefficient as a function of lift coefficient for W_3H_2 and W_2H_2 (data from reference 1) to illustrate the effect of the elevator horn balance. Figure 24 presents the variation of critical Mach number with lift coefficient for W_2 and W_3. Figure 24 also shows the variation with Mach number of the minimum pressure coefficient at the tail intersections of H_3, H_4, and H_5. Figures 25, 26, and 27 present tuft pictures to indicate the flow over the wings and tails investigated.

RESULTS AND DISCUSSION

Comparison of Wings

Lift and drag.- In figure 15, the variations with Mach number of lift-curve slope and of maximum lift-to-drag ratio are compared for W_3H_4 and W_4H_4. No pronounced advantage of one wing over the other is indicated, although the lift-curve slope is slightly greater for W_4H_4. This is explained by the fact that, while the area of W_4 was greater than that of W_3, the data for both W_3 and W_4 have been computed using the area of wing W_3. Figure 16 presents the variation with Mach number of angle of attack for several constant values of lift coefficient for the two wings (W_3 and W_4) tested with H_4. This comparison shows that there was only a small variation of the angle of attack for zero lift for both wings over the test range of Mach numbers.

The variations with Mach number of the drag coefficients at several lift coefficients for the same two wings in combination with H_4 are shown in figure 17. There was little difference in the Mach numbers of drag divergence, but the drag of W_4 was somewhat lower than that for W_3 at the highest Mach numbers, probably because of the reduced thickness-to-chord ratio and smaller trailing-edge angle of W_4.

Pitching moment.- The tail-off pitching-moment characteristics for W_3 and W_4 shown in figure 6 are presented in cross-plotted form in Figure 18. The curves for 0.2 lift coefficient in figures 18(a) and 18(b) show a reduction of pitching-moment coefficient with increasing Mach number starting at approximately 0.75 Mach number, followed by an abrupt increase in pitching-moment coefficient starting at 0.825 Mach number for W_3 and 0.85 Mach number for W_4. In the Mach number range from 0.75 to 0.85, the tail-off pitching-moment coefficient of W_4 at a lift coefficient of 0.2 varied from 0 to −0.04, while the pitching-moment coefficient of W_3 varied from 0 to −0.02. This smaller range of pitching-moment-coefficient values indicates that W_3 is somewhat superior to W_4 in this respect.

Comparison of Tails

Figure 19 shows the variation with Mach number of the tail-on pitching-moment coefficient at several lift coefficients for W_4H_4. At positive lift coefficients there was a pronounced reduction in pitching-moment coefficient with increasing Mach number in the range from about 0.75 to 0.85 Mach number. This undesirable trim change would produce a pitching-down tendency of sufficient magnitude to rule out W_4H_4 as a practical combination for the airplane. Figure 20 compares the pitching-moment characteristics for W_3H_2, W_3H_3, W_3H_4, and W_3H_5. Figures 20(b) and 20(c) indicate that excessive trim changes occurred above 0.75 Mach number with H_4 and H_5. Horizontal tail H_3 is the best of the thinner sections tested as far as the pitching-moment characteristics are concerned, and further improvement would probably be possible by suitable adjustment of the tail incidence angle. The incidence angles of H_2 and H_3 differed

by 1°, which accounts for the difference in the values of the pitching-moment coefficients for H_2 and H_3 at the lower Mach numbers. The bump at 0.80 Mach number in the curve for W_3H_2 in figure 20(b) for a model lift coefficient of 0.2 may be attributed to the nonlinearity of the lift characteristics of H_2 near its zero-lift condition. (The results presented in reference 1 indicated the Mach number of lift divergence for H_2 was approximately 0.75.)

A comparison between the tail-off and the tail-on pitching-moment-coefficient curves indicates that the various tail configurations were operating at considerably different angles of attack under the test conditions. This is borne out in figure 21, which presents the estimated elevator deflection required to maintain level flight at sea level and at 20,000 feet. An outstanding choice between the various tail locations is not readily apparent, although H_3 offers the most favorable variation of elevator deflection with Mach number.

The variations of the neutral point and of the elevator-effectiveness parameter with Mach number are shown in figure 22. A minimum value of static longitudinal stability was measured with W_3H_2, the neutral point being at the 26.5-percent point of the mean aerodynamic chord at 0.75 Mach number. The static longitudinal stability increased considerably at the higher Mach numbers for all wing and tail combinations tested, the neutral point for W_3H_5 assuming a rearward location of 60 percent of the mean aerodynamic chord at 0.90 Mach number. In figures 12(h) and 12(i), static longitudinal instability is indicated for the model with W_3H_3 at negative lift coefficients for Mach numbers above 0.825. The elevator-effectiveness parameter was considerably reduced at the higher Mach numbers, but W_3H_3 demonstrated less variation with Mach number than the other configurations. The differences in the elevator-effectiveness parameters shown in figure 22(b) were probably caused to a large extent by the differences in the downwash at the various horizontal-tail locations.

Figure 23 presents the variation of elevator hinge-moment coefficient with lift coefficient for H_2 with and without the horn balance. The horn balance produced a large effect on the variation of the elevator hinge-moment coefficient with model lift coefficient, particularly noticeable at the highest test Mach numbers.

Pressure Distribution

Figure 24(a) presents the variation of critical Mach number on the upper surface of the wing with lift coefficient for W_2 and W_3, at a wing station 17.41 inches laterally from the fuselage center line. The variations of minimum peak pressure coefficient with Mach number for the H_3, H_4, and H_5 tail intersections are shown in figure 24(b). The midchord critical Mach number for W_3 was slightly greater over the entire lift-coefficient range than for W_2 but the leading-edge critical Mach number was considerably less. The result of displacing the horizontal tail relative to the vertical tail, as indicated by the minimum peak pressure coefficients, is shown in figure 24(b). Moving the horizontal tail rearward or downward and rearward increased the critical Mach number at the intersection.

Tuft Studies

The photographs of tufts on the model presented in figures 25(a) through 25(d) compare the flow over W_3 and W_4 at 0.775 and 0.825 Mach numbers at angles of attack of 2° and 0°. These photographs indicate that the pitching-down tendencies of the two wings (discussed in connection with fig. 18) were not caused by separation from the wing. Figures 25(e) through 25(h), which present additional pictures of tufts on the model for Mach numbers of 0.85 and 0.875 at 2° angle of attack, show pronounced separation over both wings and indicate that the marked climbing tendencies of W_3 and W_4 shown in figure 18 were apparently caused by the separation. Further information on this subject is presented in reference 2. The extent of the separation at 0.85 and 0.875 Mach numbers indicates that the airplane would probably experience severe buffeting. Figure 26 presents photographs of tufts on the model for the three horizontal tails (H_3, H_4, and H_5). The picture of H_4 shown in figure 26(b) indicates a small amount of separation at the root section of the trailing edge. The tufts on H_5 shown in figure 26(c) indicate an improvement in the flow at the intersection even though H_5 was operating at a larger tail angle of attack than H_3 or H_4. The two fairings tested in attempts to improve the flow at the tail intersection with tails H_2 and H_3 did not produce any perceptible improvement in the flow characteristics. Figure 27 includes photographs of tufts on horizontal tail H_2 with and without the fairings at a Mach number of 0.85.

CONCLUSIONS

The conclusions drawn from the high-speed wind-tunnel tests of the modified 0.17-scale model of the XF2H-1 airplane were as follows:

1. The comparisons between the results for the model having the 11- and 9-percent-thick tail assemblies indicate that the use of the thinner section reduced the variation of the pitching-moment coefficient with Mach number.

2. Rearward or rearward and downward displacements of the horizontal tail improved the flow at the intersection, but resulted in an excessive change in pitching-moment coefficient at the higher Mach numbers.

3. The extension of the trailing edge of the wing increased the Mach number at which the pitching-up tendency developed from 0.825 to 0.85, but increased the pitching-down tendency between 0.75 and 0.825 Mach numbers.

Ames Aeronautical Laboratory,
National Advisory Committee for Aeronautics,
Moffett Field, Calif.

REFERENCES

1. Axelson, John A., and Emerson, Horace F.: High-Speed Stability and Control Characteristics of a 0.17-Scale Model of the McDonnell XF2H-1 Airplane (TED No. NACA DE 318). NACA RM SA9C31, 1949.

2. Axelson, John A., and Eley, Herman O.: Effects of Mach Number on the Spanwise Load Distribution and Aerodynamic Characteristics of the Wing of the McDonnell XFD-1 Airplane Predicted from Wind-Tunnel Tests (TED No. 2310). NACA ~~RM~~ A6A23, 1946.

FIGURE LEGENDS

Figure 1.– Wing plan forms tested on the 0.17-scale model of the McDonnell XF2H-1 airplane.

Figure 2.– Geometric characteristics of wings W_3 and W_4.

Figure 3.– Side view of the vertical tail with the locations of H_2, H_3, H_4, and H_5.

Figure 4.– The 0.17-scale McDonnell XF2H-1 model mounted on the sting-support system in the Ames 16-foot high-speed wind tunnel. (a) Model with W_3H_3. (b) Model with W_3H_5.

Figure 5.– Drag polars at various Mach numbers for the model without tail surfaces. (a) W_3. (b) W_4.

Figure 6.– Variation of pitching-moment coefficient with lift coefficient at various Mach numbers for the model without tail surfaces. (a) W_3. (b) W_4.

Figure 7.– Lift curves at various Mach numbers for the model without tail surfaces. (a) W_3. (b) W_4.

Figure 8.– Drag Polars for the complete model at various Mach numbers. (a) W_3H_4. (b) W_4H_4.

Figure 9.– Variation of pitching-moment coefficient with lift coefficient for the complete model at various Mach numbers. (a) W_3H_4. (b) W_4H_4.

Figure 10.– Lift curves for the complete model at various Mach numbers. (a) W_3H_4. (b) W_4H_5.

Figure 11.– Variation of pitching-moment coefficient with lift coefficient for W_3H_2 at various Mach numbers. i_t, 1°.

Figure 12.– Variation of pitching-moment coefficient with lift coefficient for W_3H_3 at various elevator deflections and Mach numbers. i_t, 0°. (a) M, 0.40. (b) M 0.60.

Figure 12.– Continued. (c) M, 0.70. (d) M,0.75.

Figure 12.– Continued. (e) M, 0.775. (f) M, 0.80.

Figure 12.– Continued. (g) M, 0.825. (h) M, 0.85.

Figure 12.– Concluded. (i) M, 0.875. (j) M, 0.90.

Figure 13.– Variation of pitching-moment coefficient with lift coefficient for W_3H_4 at various elevator deflections and Mach numbers. i_t, 0°. (a) M, 0.40. (b) M, 0.60.

Figure 13.– Continued. (c) M, 0.70. (d) M, 0.75.

Figure 13.– Continued. (e) M, 0.775. (f) M, 0.80.

Figure 13.– Continued. (g) M, 0.825. (h) M, 0.85.

Figure 13.– Concluded. (i) M, 0.875. (j) M, 0.90.

Figure 14.– Variation of pitching-moment coefficient with lift coefficient for W_3H_5 at various elevator deflections and Mach numbers i_t, 0°. (a) M, 0.40. (b) M, 0.60.

Figure 14.– Continued. (c) M, 0.70. (d) M, 0.75.

Figure 14.– Continued. (e) M, 0.775. (f) M, 0.80.

Figure 14.– Continued. (g) M, 0.825. (h) M, 0.850.

Figure 14.– Concluded. (i) M, 0.875. (j) M, 0.90.

Figure 15.– Variation with Mach number of lift-curve slope and maximum lift-to-drag ratio for W_3H_4 and W_4H_4. δ_e, 0°.

Figure 16.– Variation with Mach number of angle of attack at several lift coefficients for W_3H_4 and W_4H_4. (a) W_3H_4. (b) W_4H_4.

Figure 17.– Variation with Mach number of drag coefficient at several lift coefficients for W_3H_4 and W_4H_4.

Figure 18.– Variation with Mach number of pitching-moment coefficient at several lift coefficients for the model without tail surfaces. (a) W_3. (b) W_4.

Figure 19.– Variation with Mach number of pitching-moment coefficient at several lift coefficients for W_4H_4. i_t, 0°; δ_e, 0°. (a) C_L, 0. (b) C_L, 0.2. (c) C_L, 0.4.

Figure 20.– Variation with Mach number of pitching-moment coefficient at several lift coefficients for W_3 in combination with H_2, H_3, H_4, and H_5. i_t, 0° for H_3, H_4, H_5; i_t, 1° for H_2; δ_e, 0°. (a) C_L, 0. (b) C_L, 0.2. (c) C_L, 0.04.

Figure 21.– Estimated elevator deflection required with a wing loading of 50 pounds per square foot for level flight at sea level and at 20,000 feet for W_3H_3, W_3H_4, and W_3H_5. i_t, 0°. (a) Sea level. (b) 20,000 feet.

Figure 22.- Variations of the stick-fixed neutral point and of the elevator-effectiveness parameter with Mach number for various wing and tail combinations. C_L, 0.2. (a) Neutral point, percent M.A.C. (b) Elevator-effectiveness parameter.

Figure 23.- Variation of elevator hinge-moment coefficient with lift coefficient at various Mach numbers for W_2H_2 with horn balance (data from reference 1) and for W_3H_2 without horn balance. i_t, 1°; δ_e, 0°.

Figure 24.- Experimentally determined critical Mach number for the wing and tails. (a) Critical Mach number on upper surface of wing at a lateral distance of 17.41 inches from fuselage center line. (b) Minimum peak pressure coefficient at tail intersection. Model lift coefficient, 0.2.

Figure 25.- Photograph of tufts on wings W_3 and W_4. (a) W_3. M,0.775; α_u, 2°; C_L, 0.36. (b) W_3. M, 0.825; α_u, 0°; C_L, 0.10. (c) W_4. M, 0.775; α_u, 2°; C_L, 0.30. (d) W_4. M, 0.825; α_u, 0°; C_L, 0.08.

Figure 25.- Concluded. (e) W_4. M, 0.85; α_u, 2°; C_L, 0.22. (f) W_3. M, 0.875; α_u, 2°; C_L, 0.12. (g) W_4. M, 0.85; α_u, 2°; C_L, 0.29. (h) W_4. M, 0.875; α_u, 2°; C_L, 0.23.

Figure 26.- Photographs of tufts on horizontal tails H_3, H_4, and H_5 tested with wing W_3. (a) H_3. M, 0.85; α_u, 2°; C_L, 0.17. (b) H_4. M, 0.85; α_u, 2°; C_L, 0.24. (c) H_5. M, 0.85; α_u, 2°; C_L, 0.25.

Figure 27.- Photographs of tufts on horizontal tail H_2 tested with wings W_2 and W_3. (a) W_2H_2. M, 0.85; α_u, 2°; C_L, 0.12 (from reference 1). (b) W_3H_2 with bullet fairing. M, 0.85; α_u, 2°; C_L, 0.22. (c) W_3H_2 with hourglass fairing. M, 0.85; α_u, 2°; C_L, 0.22.

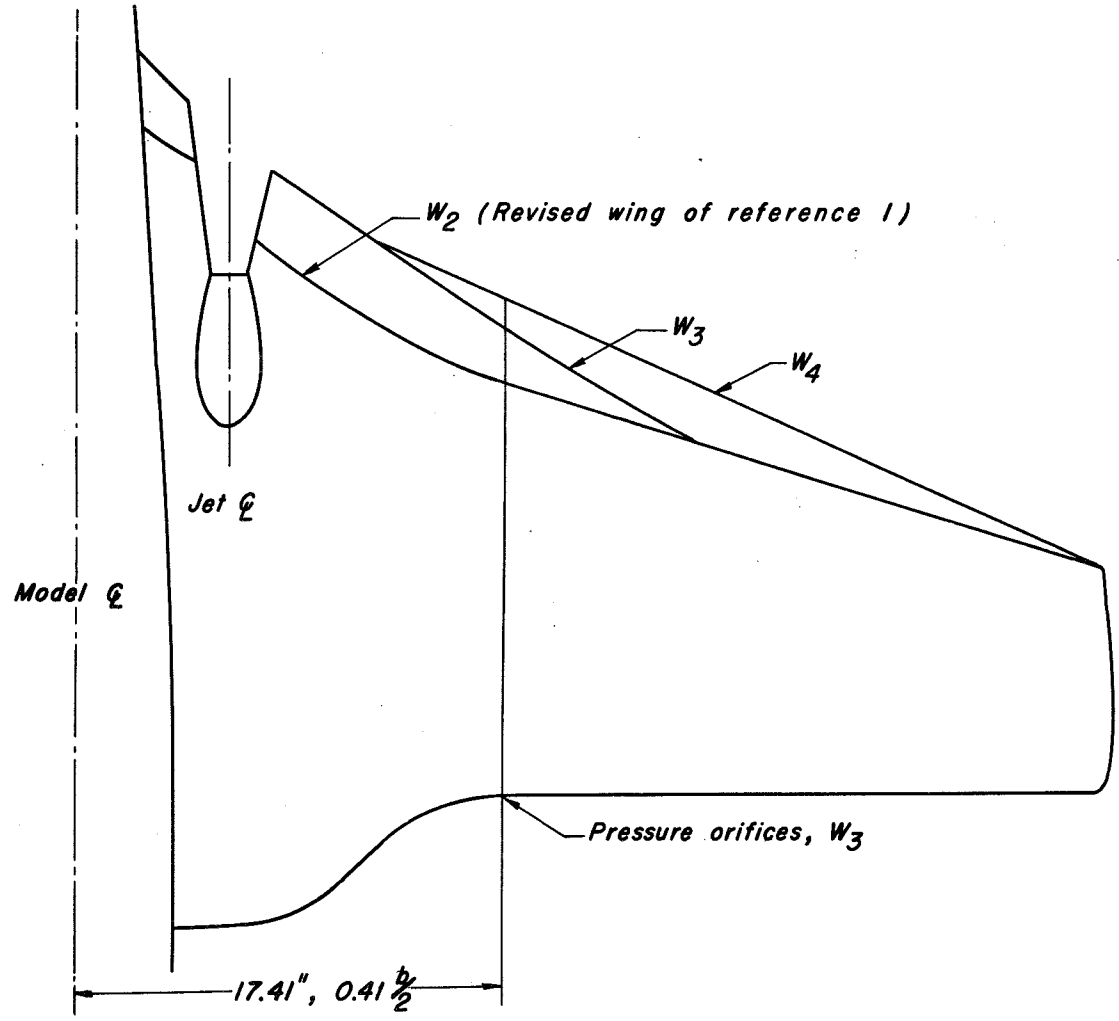

Figure 1.— Wing plan forms tested on the 0.17-scale model of the McDonnell XF2H-1 airplane.

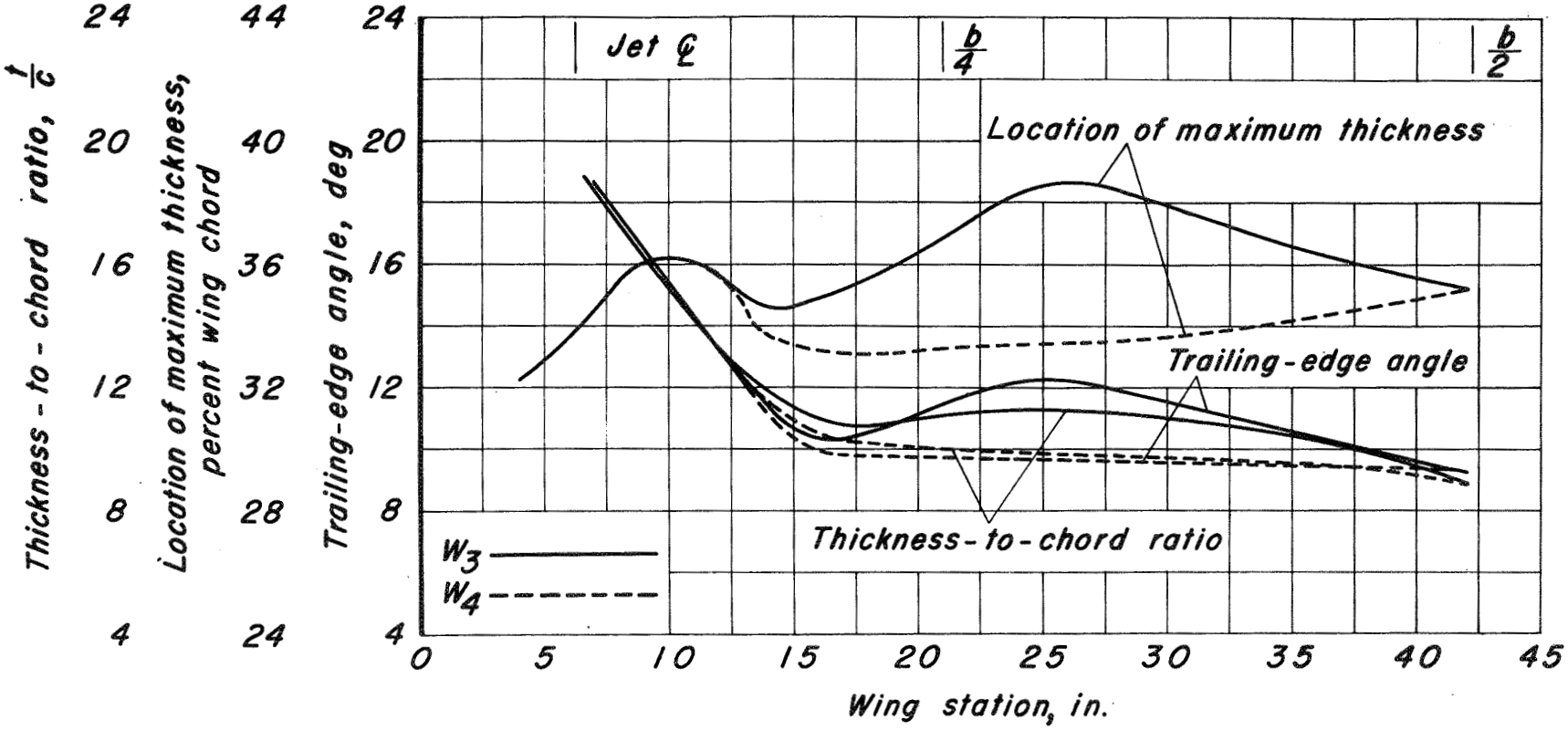

Figure 2.—Geometric characteristics of wings W_3 and W_4.

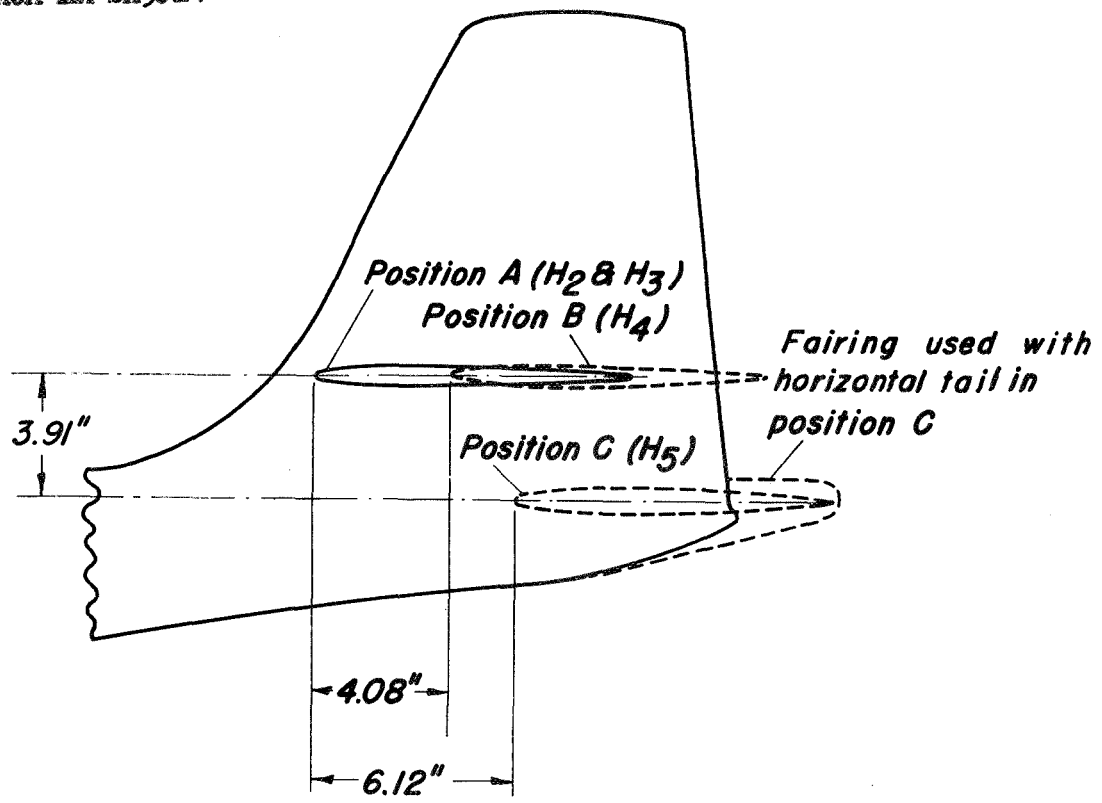

	Horizontal Tail			Vertical Tail
	NACA section	Incidence, deg	Dihedral, deg	NACA section
H_2	65-011	1	0	65-011
H_3	65-009	0	0	65-009
H_4	65-009	0	0	65-009
H_5	65-009	0	10	65-009

Figure 3.—Side view of the vertical tail with the locations of H_2, H_3, H_4, and H_5.

(a) Model with $W_3 H_3$.

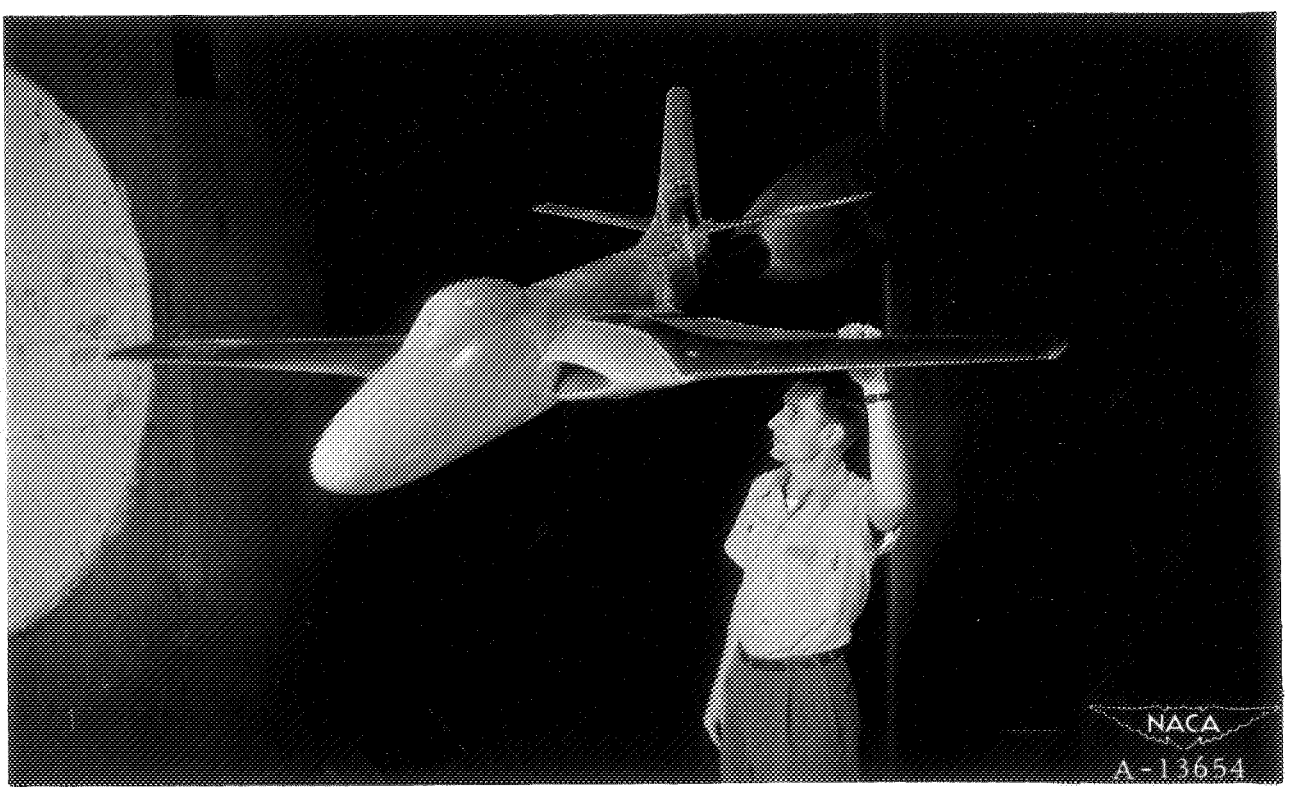

(b) Model with W_3H_5.

Figure 4.- The 0.17-scale McDonnell XF2H-1 model mounted on the sting-support system in the Ames 16-foot high-speed wind tunnel.

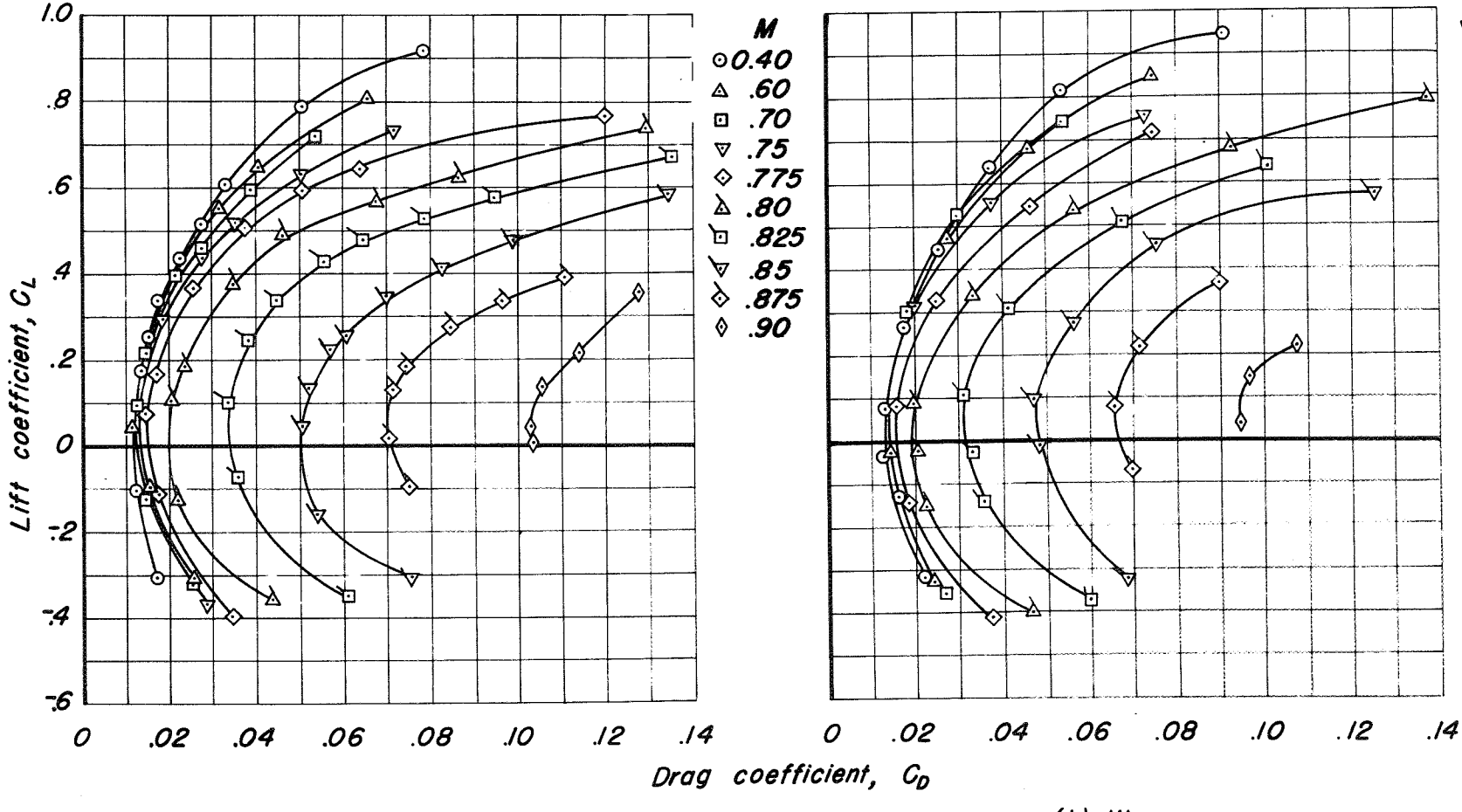

(a) W_3.

(b) W_4.

Figure 5.—Drag polars at various Mach numbers for the model without tail surfaces.

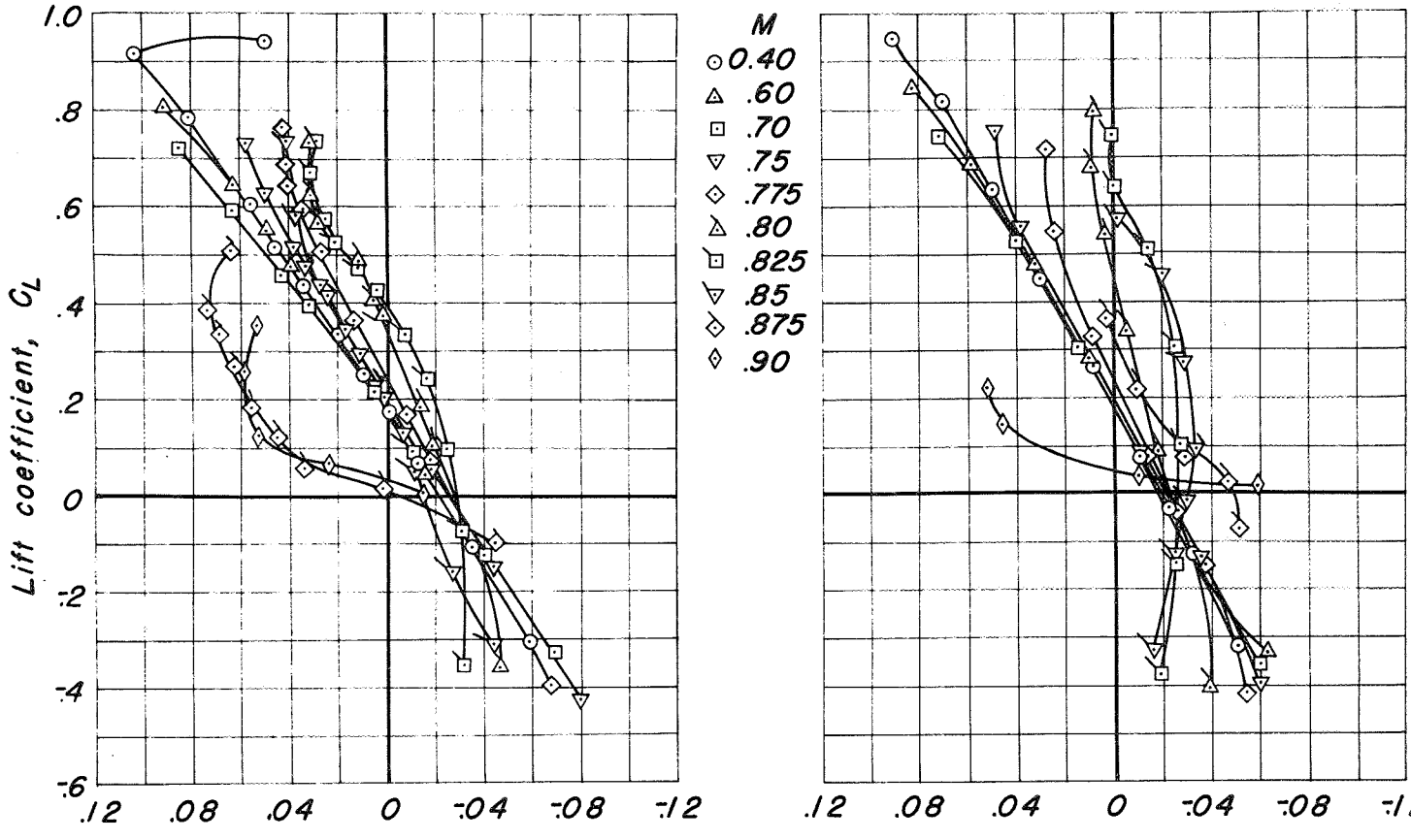

Figure 6.—Variation of pitching-moment coefficient with lift coefficient at various Mach numbers for the model without tail surfaces.

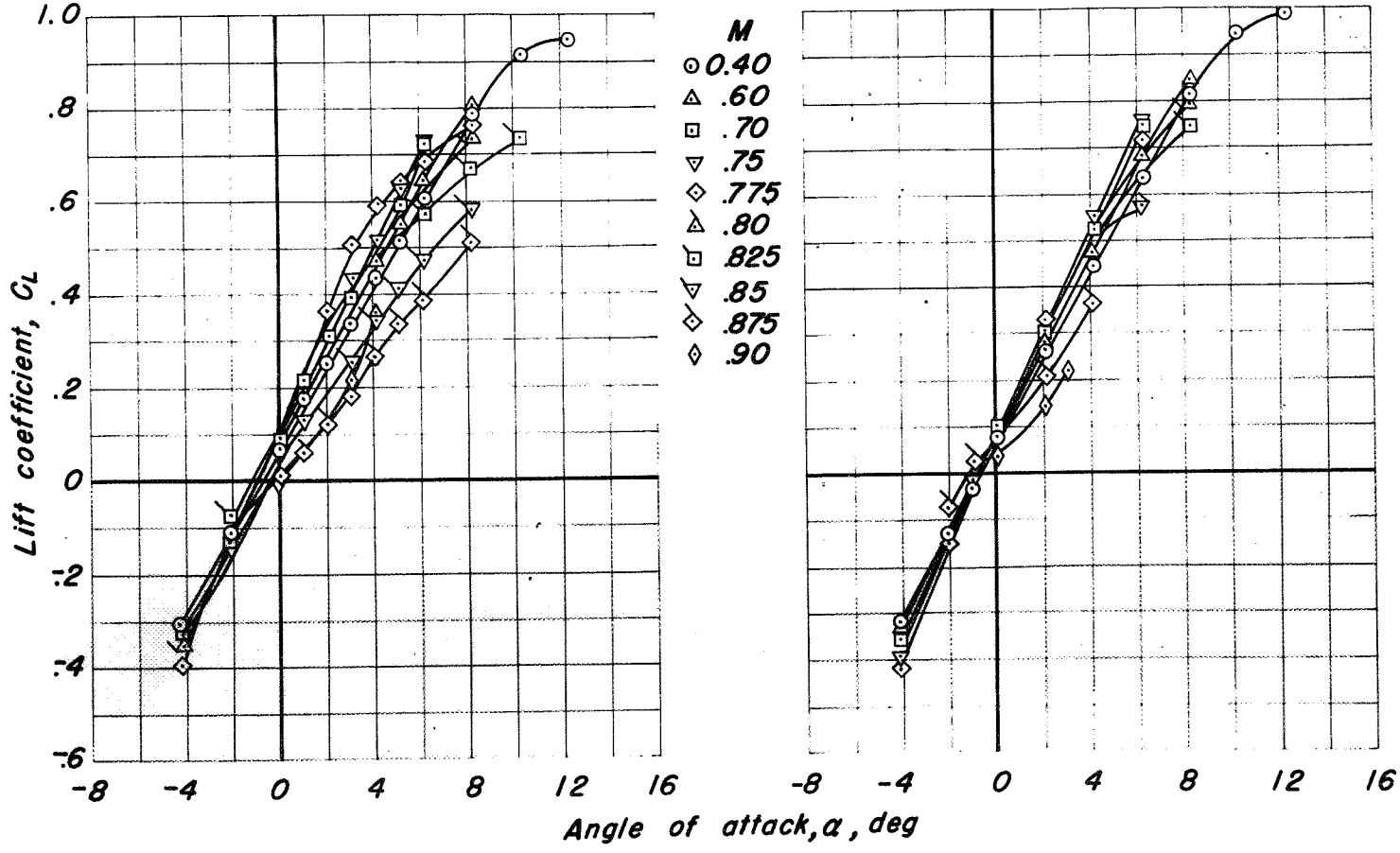

Figure 7.— Lift curves at various Mach numbers for the model without tail surfaces.

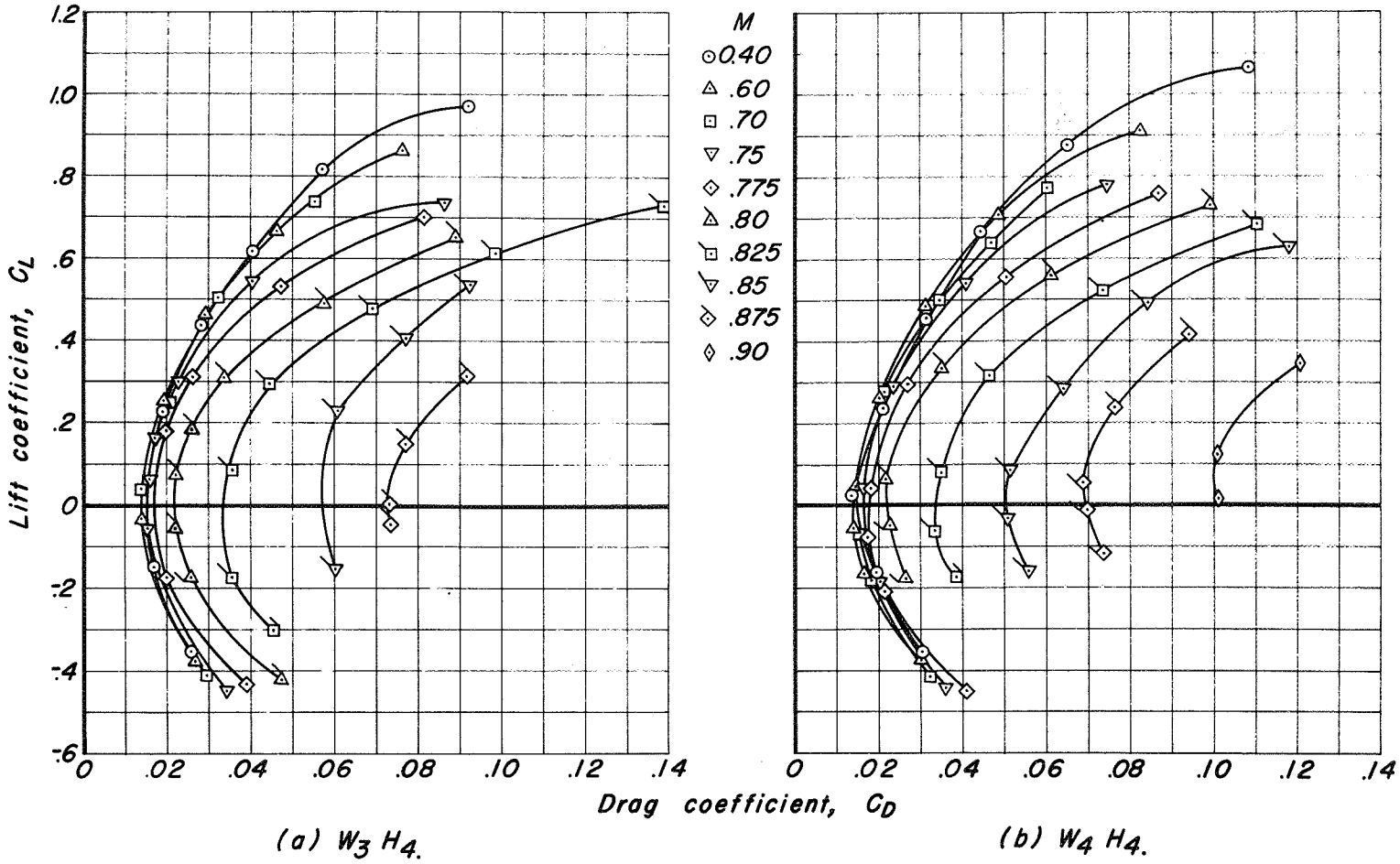

Figure 8.—Drag polars for the complete model at various Mach numbers.

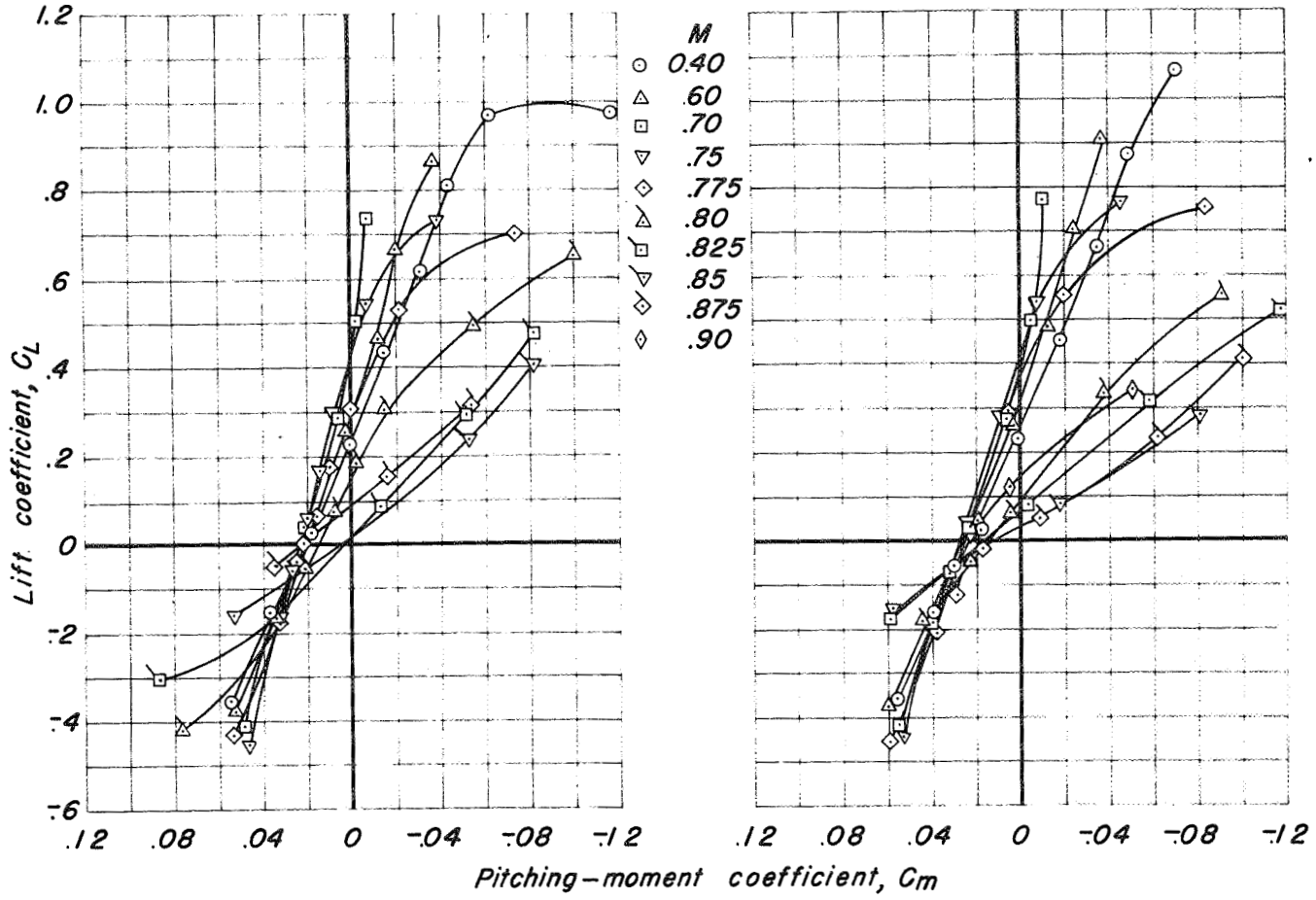

(a) W_3 H_4.

(b) W_4 H_4.

Figure 9.—Variation of pitching-moment coefficient with lift coefficient for the complete model at various Mach numbers.

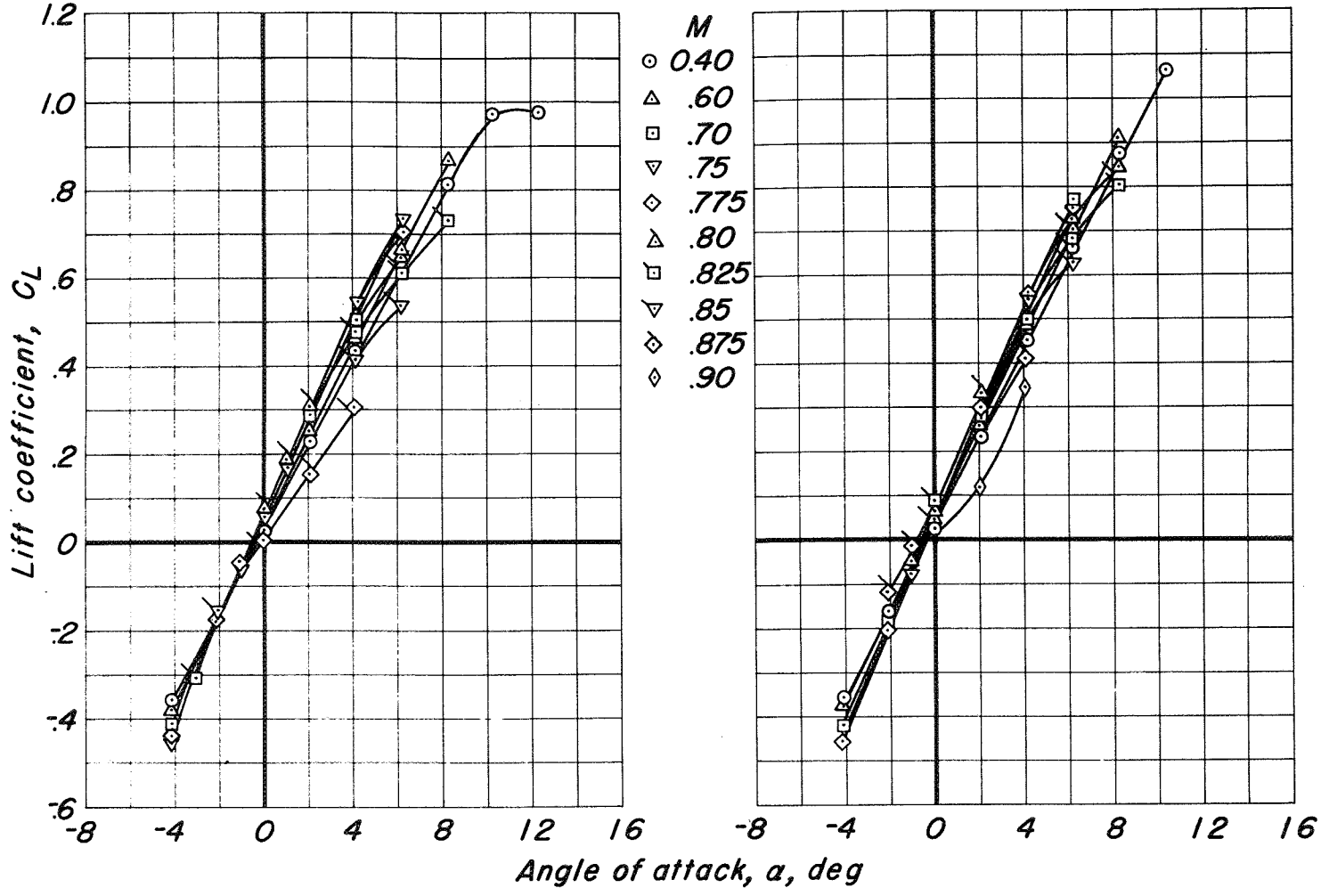

(a) W_3 H_4.

(b) W_4 H_4.

Figure 10.—Lift curves for the complete model at various Mach numbers.

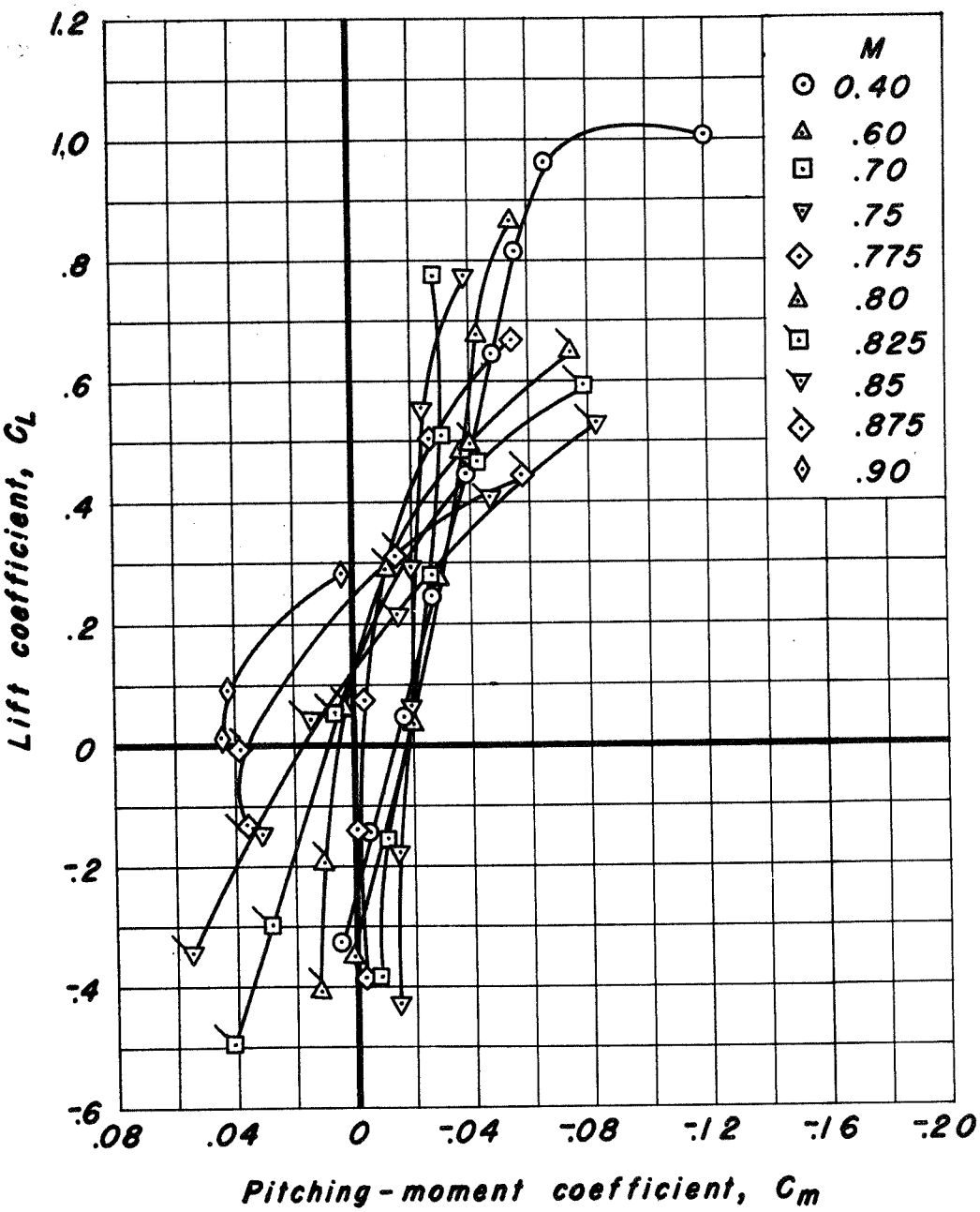

Figure 11.—Variation of pitching-moment coefficient with lift coefficient for $W_3 H_2$ at various Mach numbers. i_t, 1°.

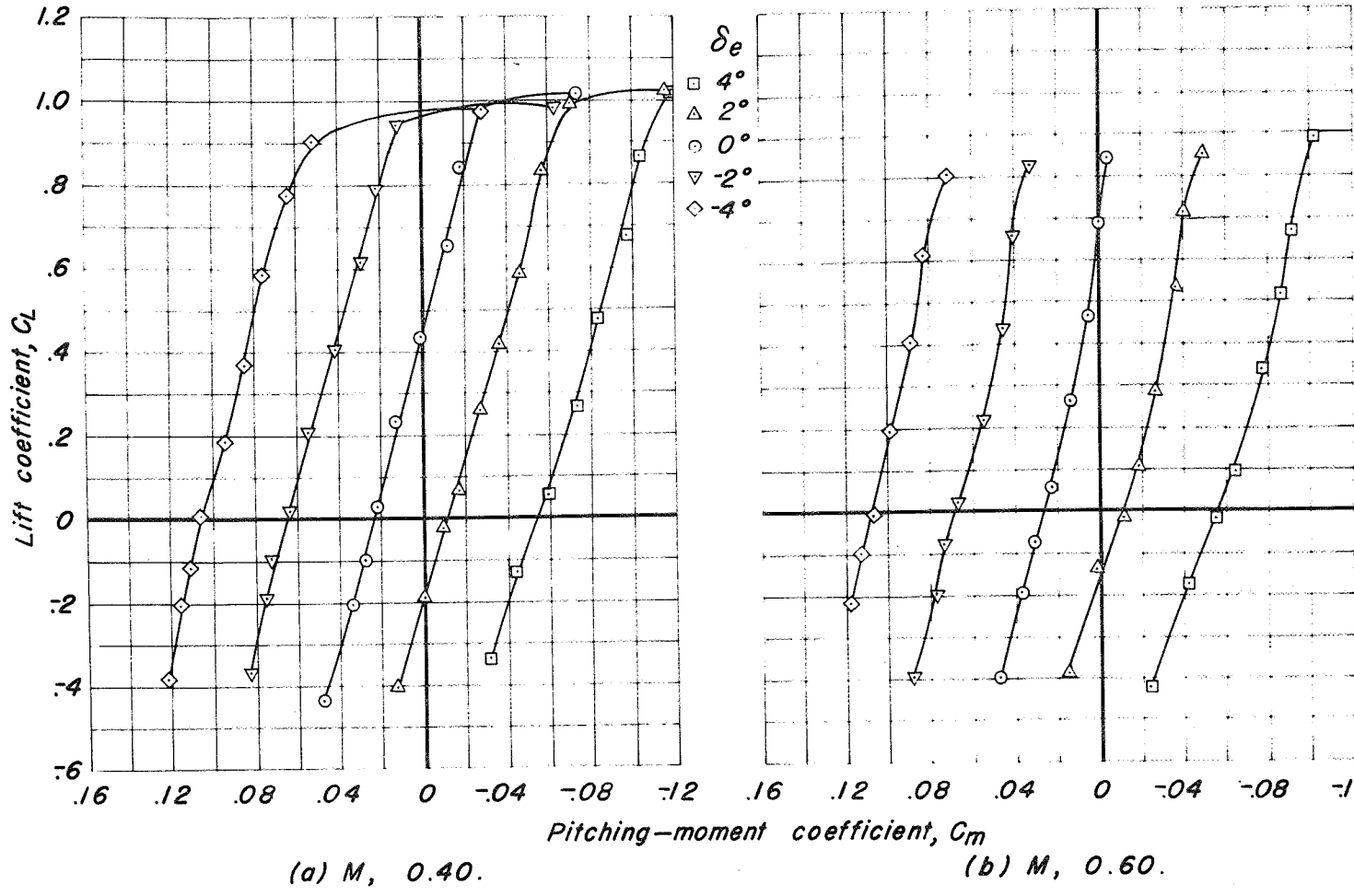

Figure 12.—Variation of pitching-moment coefficient with lift coefficient for W_3H_3 at various elevator deflections and Mach numbers. i_t, 0°.

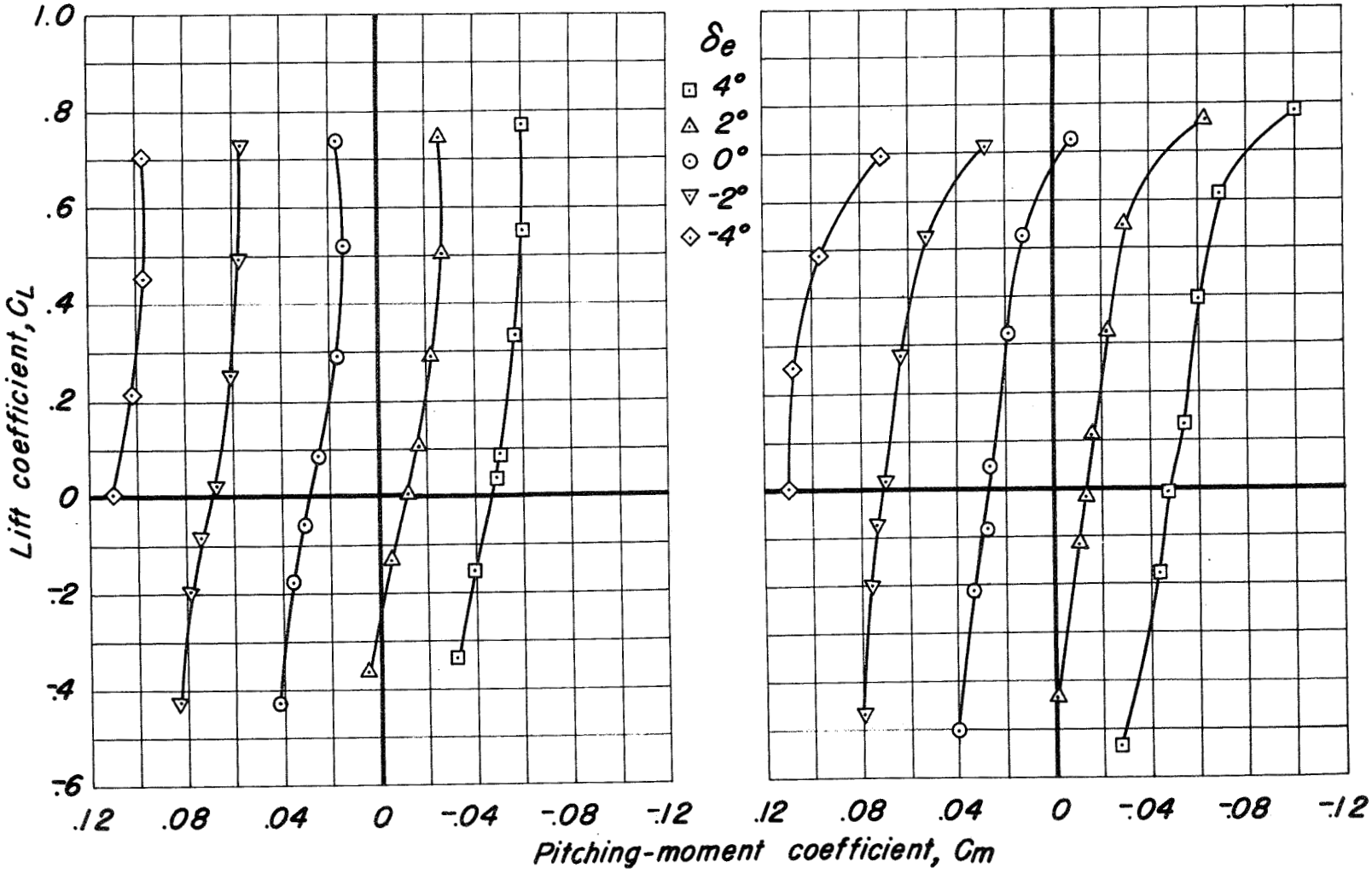

(c) M, 0.70.

(d) M, 0.75.

Figure 12.- Continued.

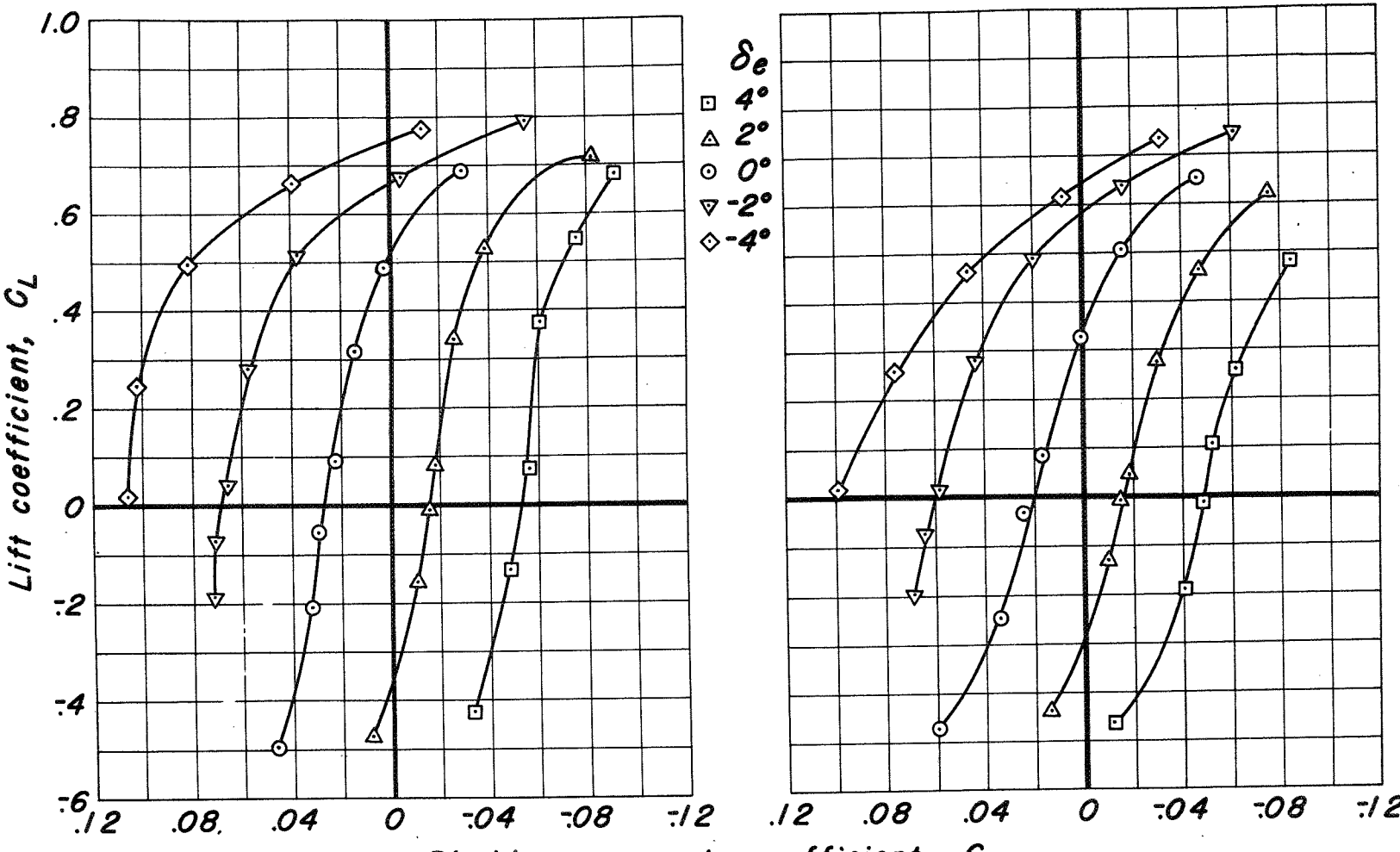

(e) M, 0.775.

(f) M, 0.80.

Figure 12.—Continued.

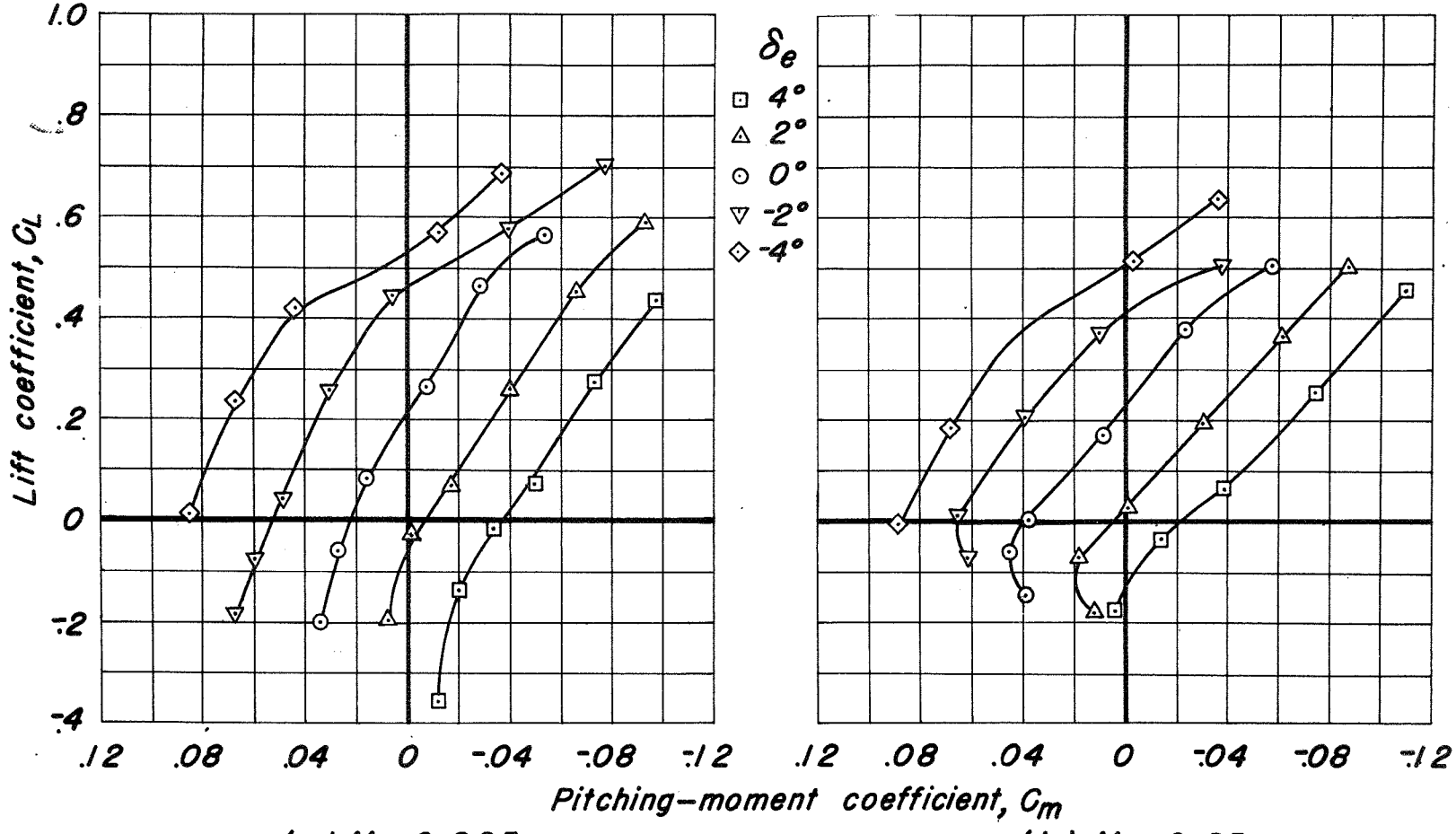

(g) M, 0.825. (h) M, 0.85.

Figure 12.- Continued.

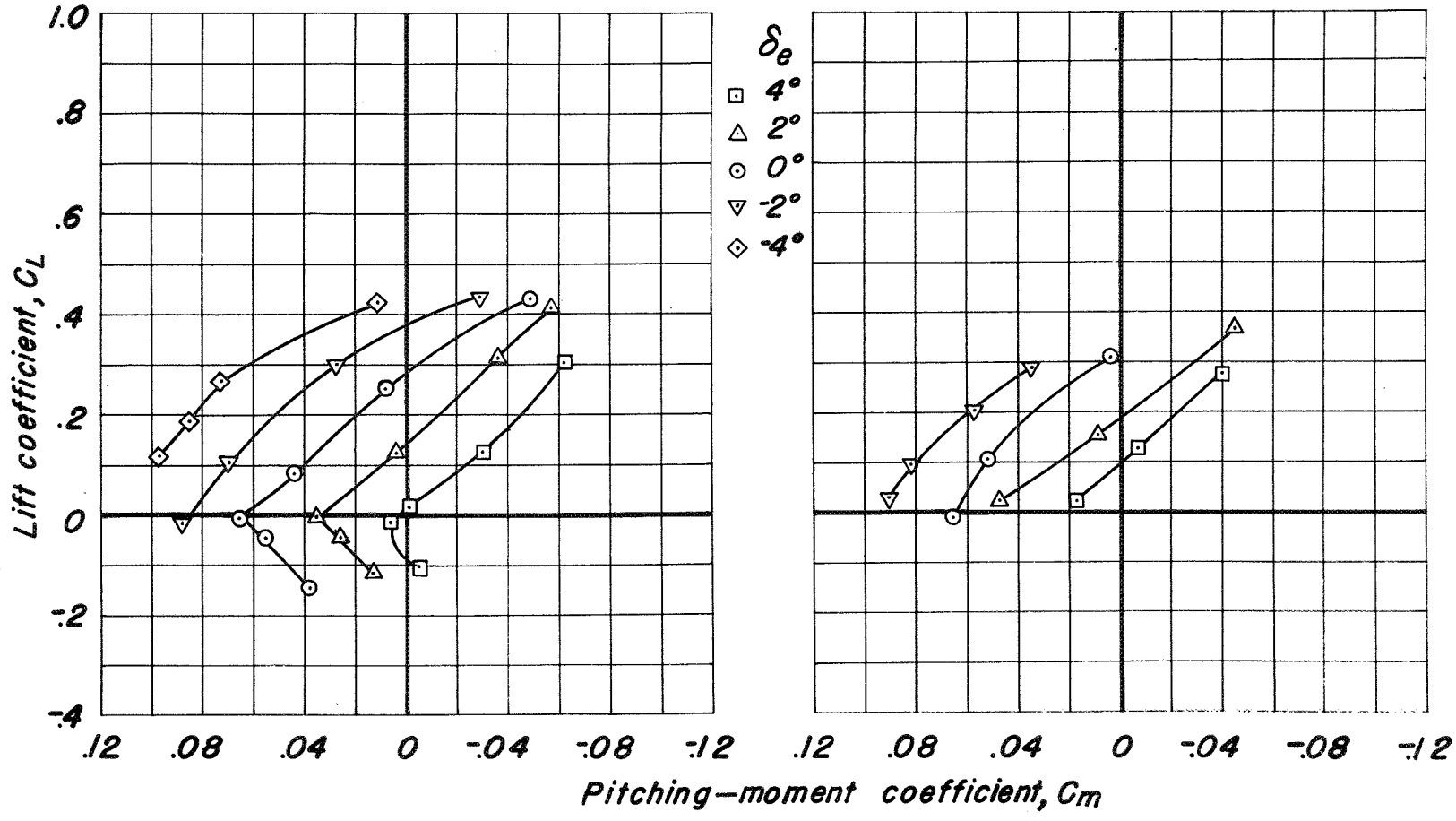

(i) M, 0.875.

(j) M, 0.90.

Figure 12.— Concluded.

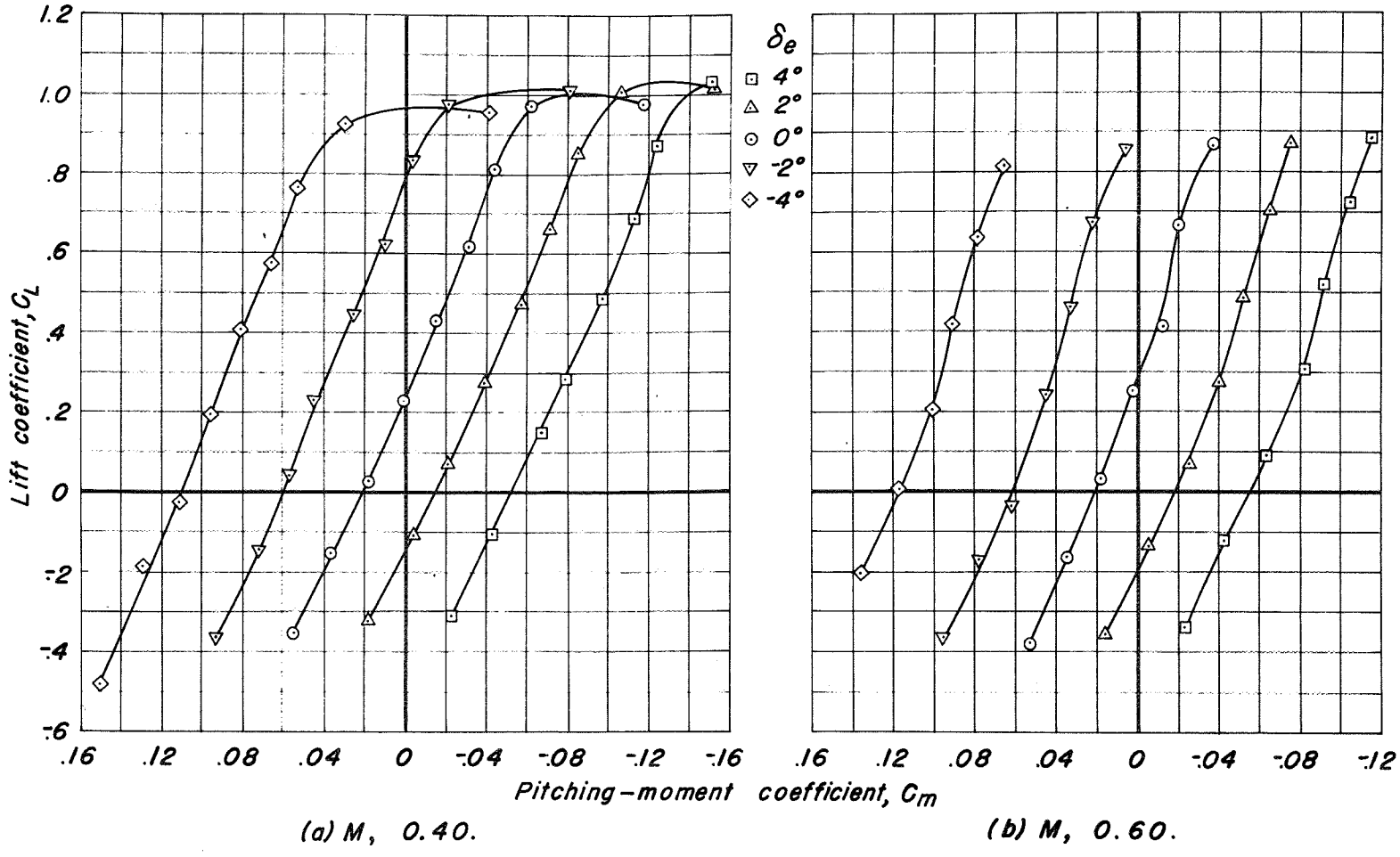

Figure 13.—Variation of pitching-moment coefficient with lift coefficient for W_3H_4 at various elevator deflections and Mach numbers. i_t, 0°.

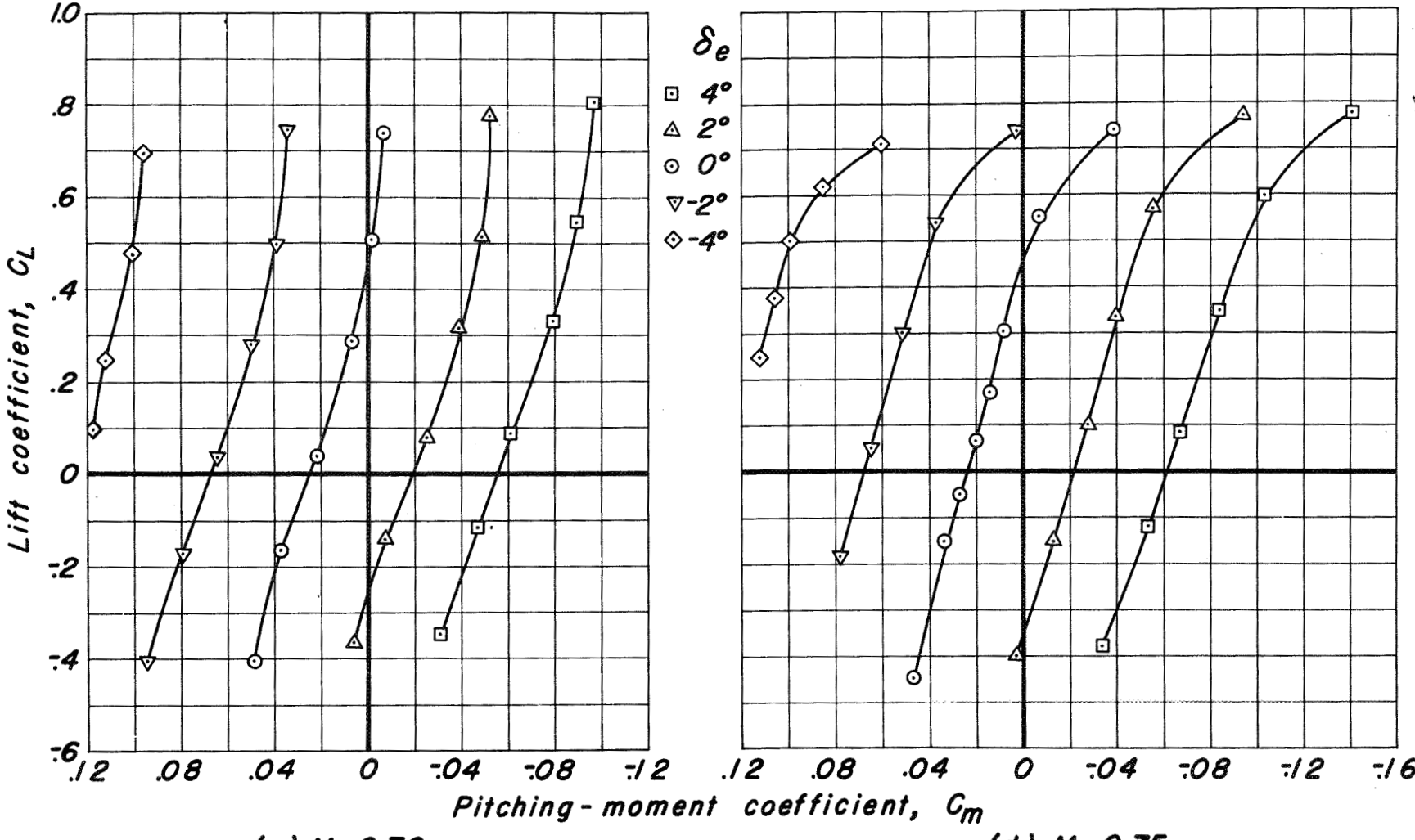

Figure 13.— Continued.

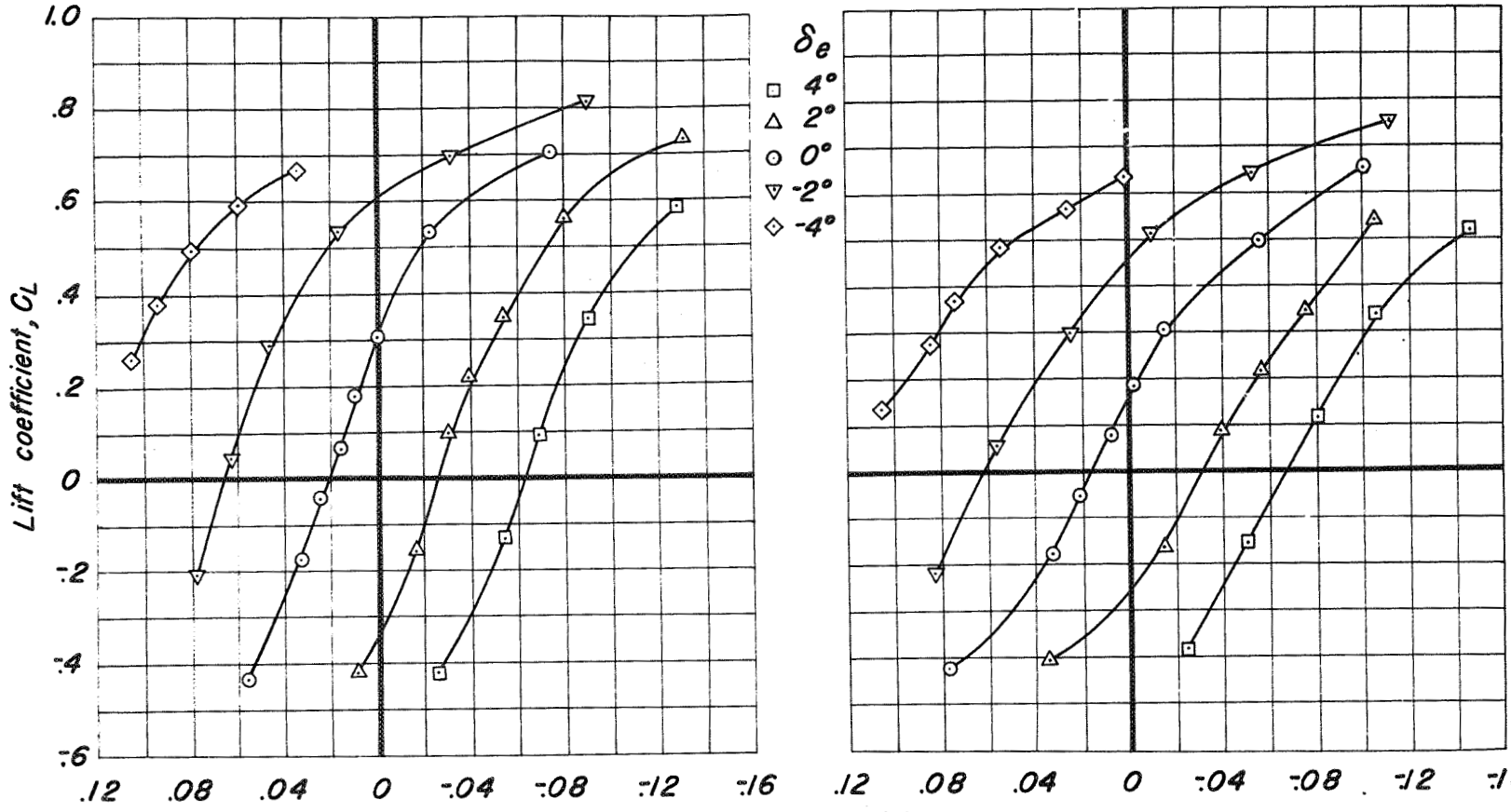

(e) M, 0.775. (f) M, 0.80.

Figure 13.- Continued.

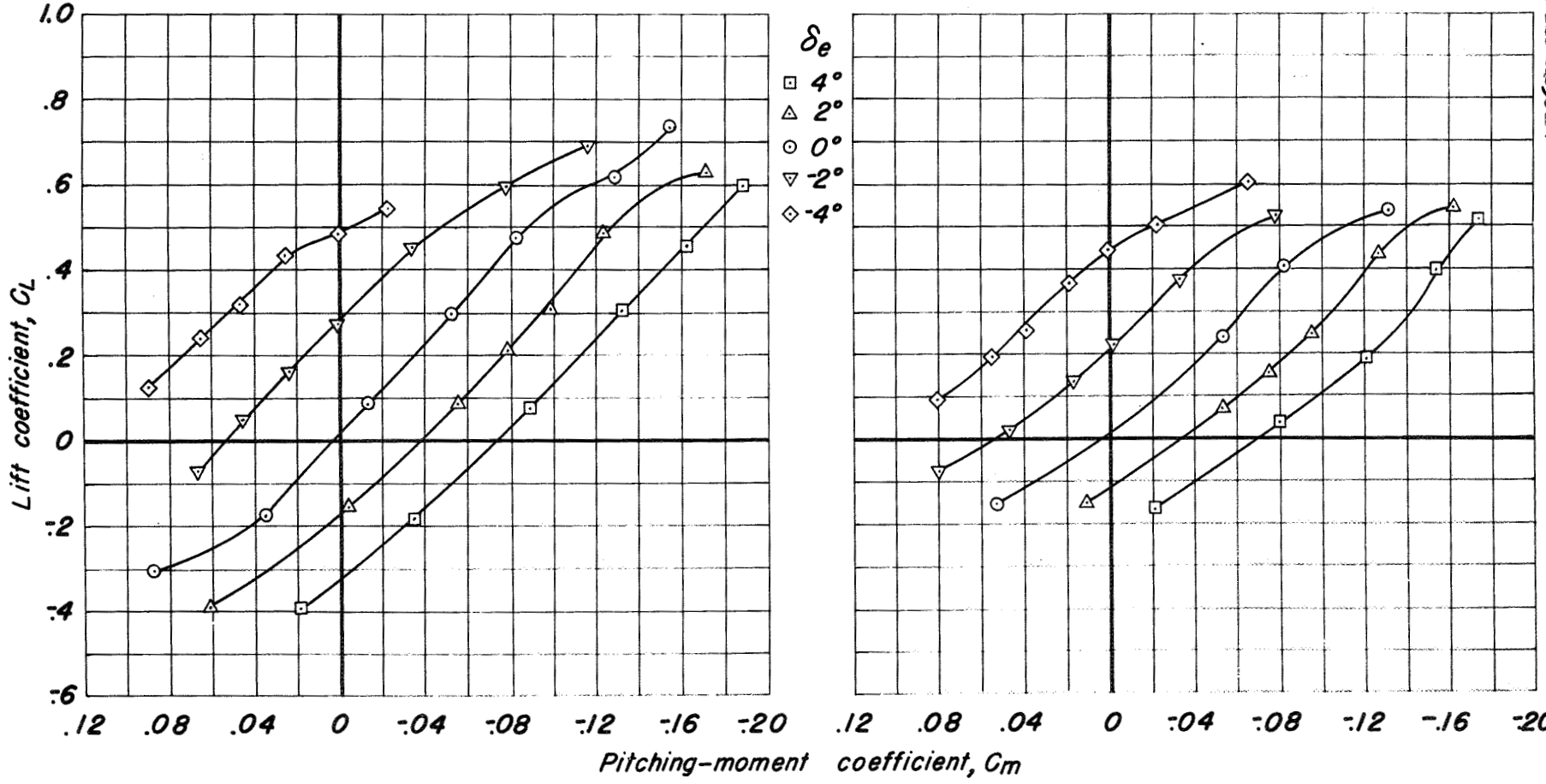

(g) M, 0.825.

(h) M, 0.85.

Figure 13.— Continued.

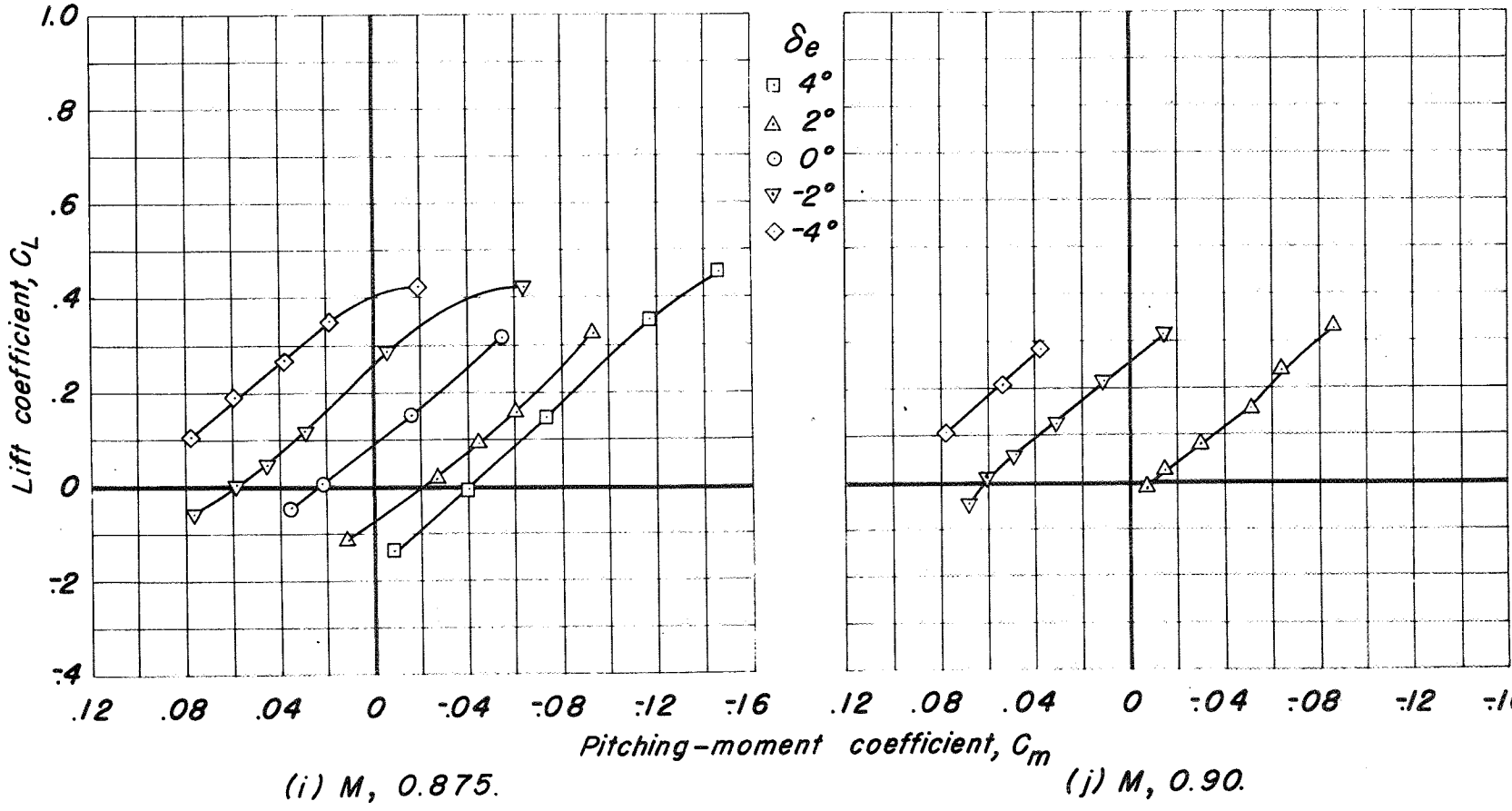

(i) M, 0.875.

(j) M, 0.90.

Figure 13.— Concluded.

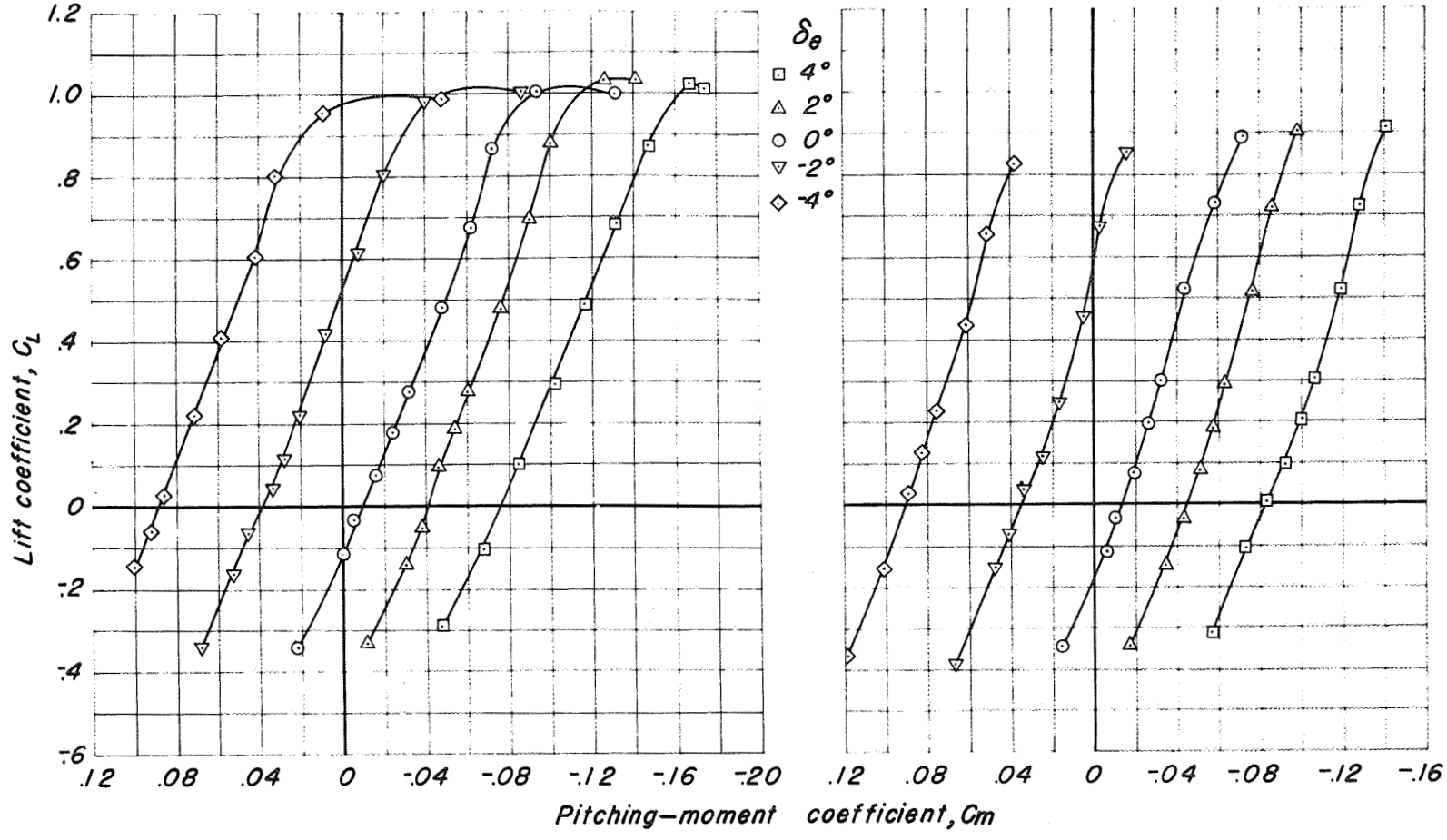

Figure 14.—Variation of pitching-moment coefficient with lift coefficient for W_3H_5 at various elevator deflections and Mach numbers. i_t, 0°.

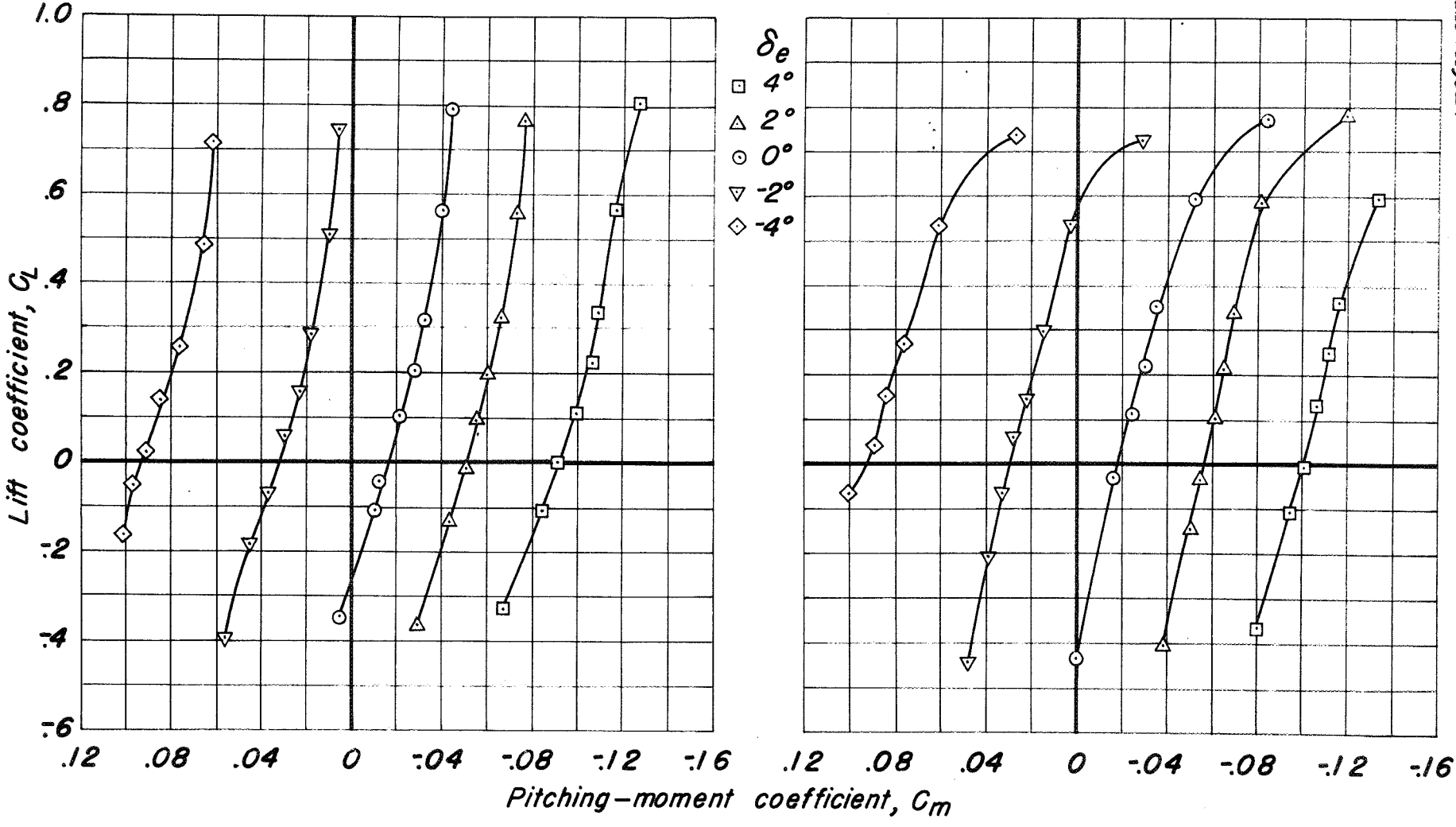

(c) M, 0.70.

(d) M, 0.75.

Figure 14.- Continued.

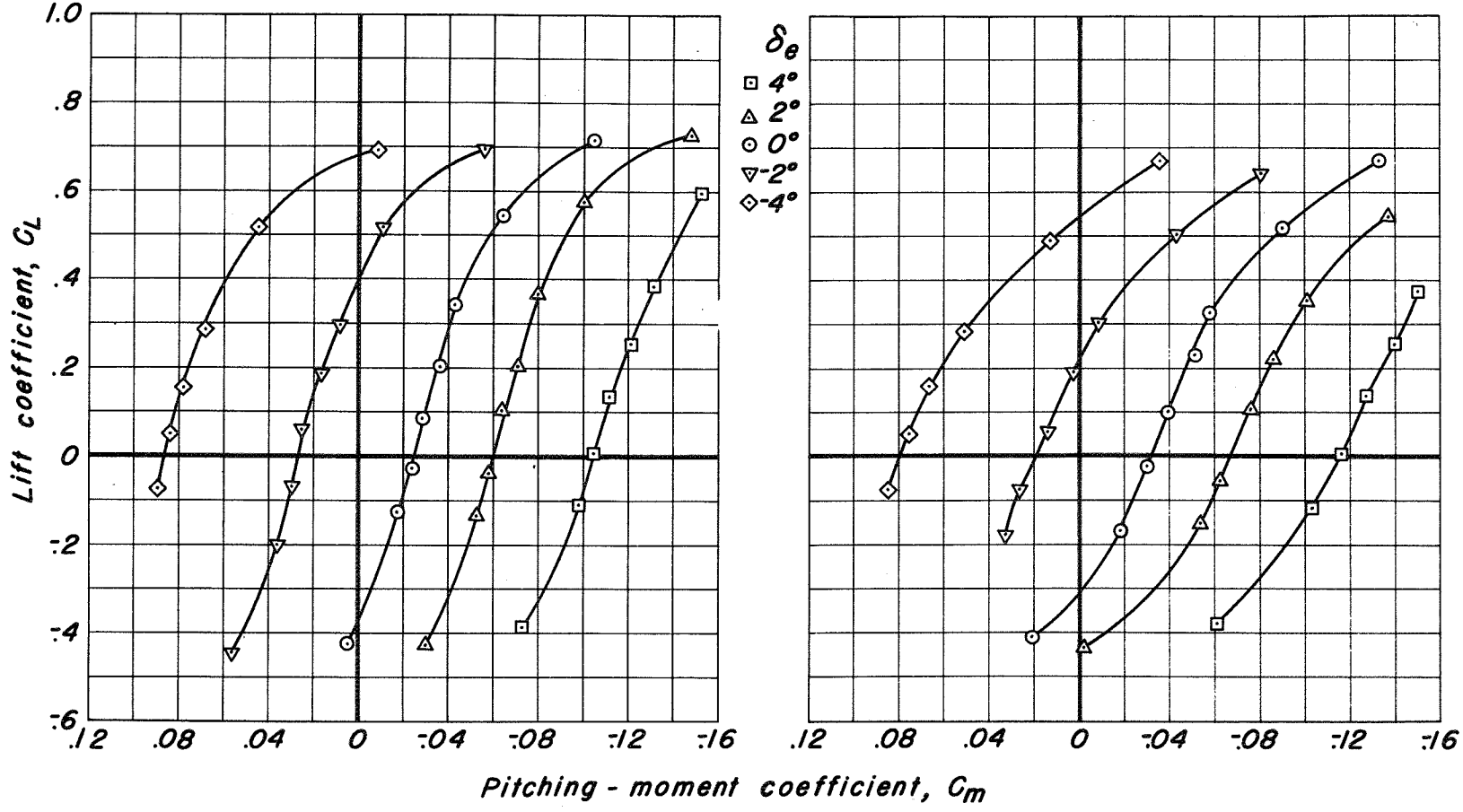

(e) M, 0.775.

(f) M, 080.

Figure 14.—Continued.

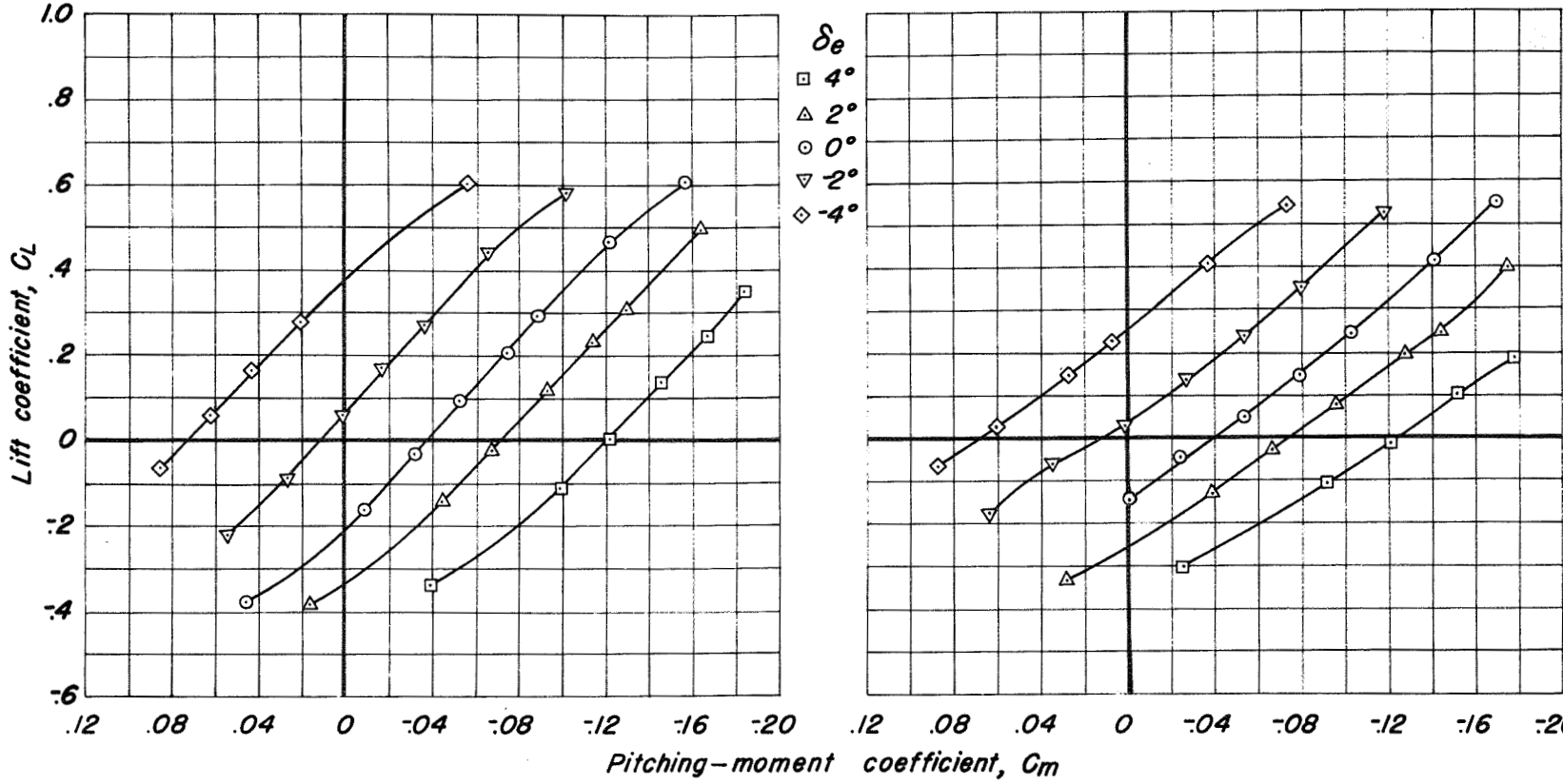

(g) M, 0.825.

(h) M, 0.850.

Figure 14.—Continued.

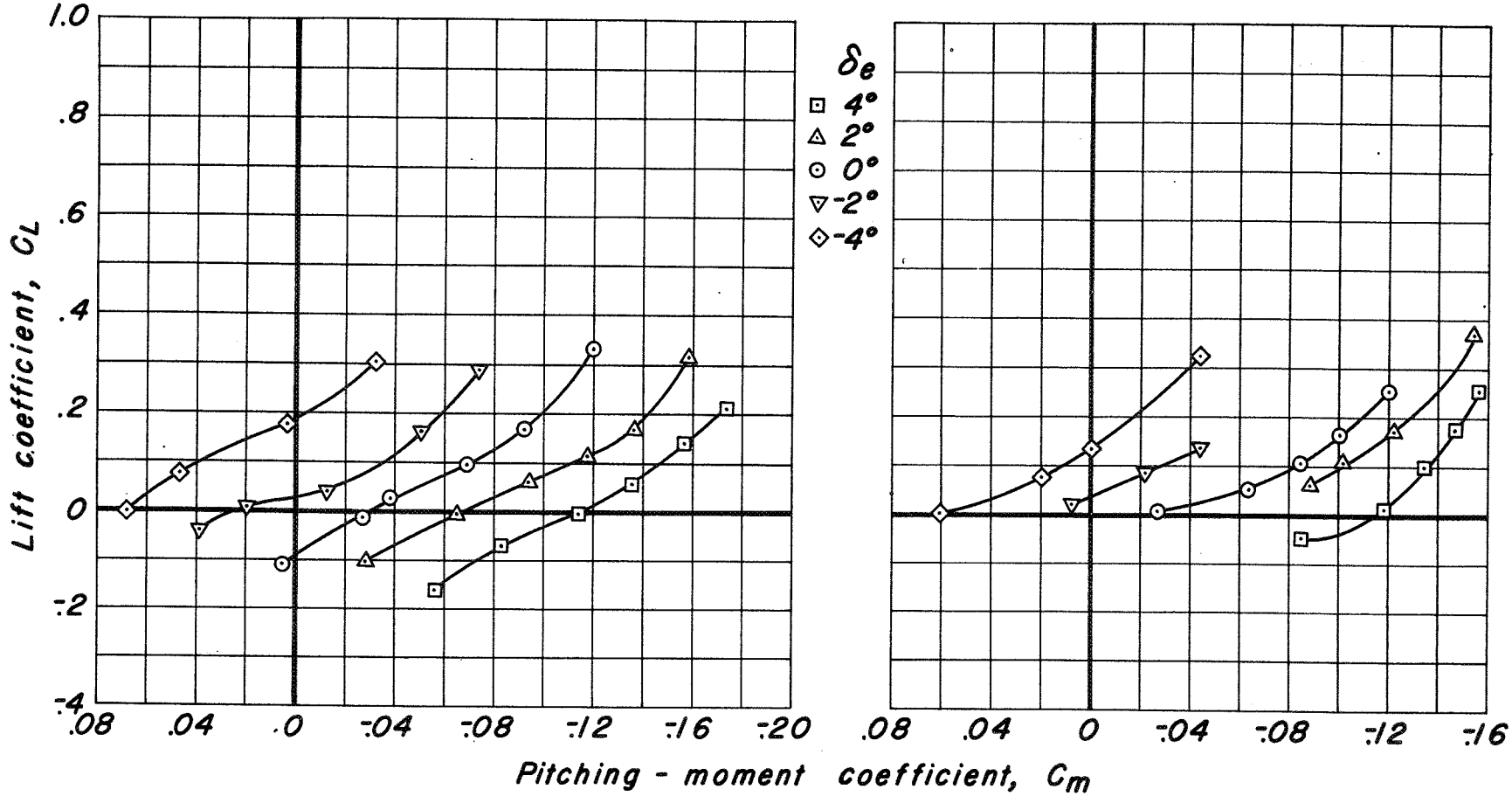

(i) M, 0.875.

(j) M, 0.90.

Figure 14.—Concluded.

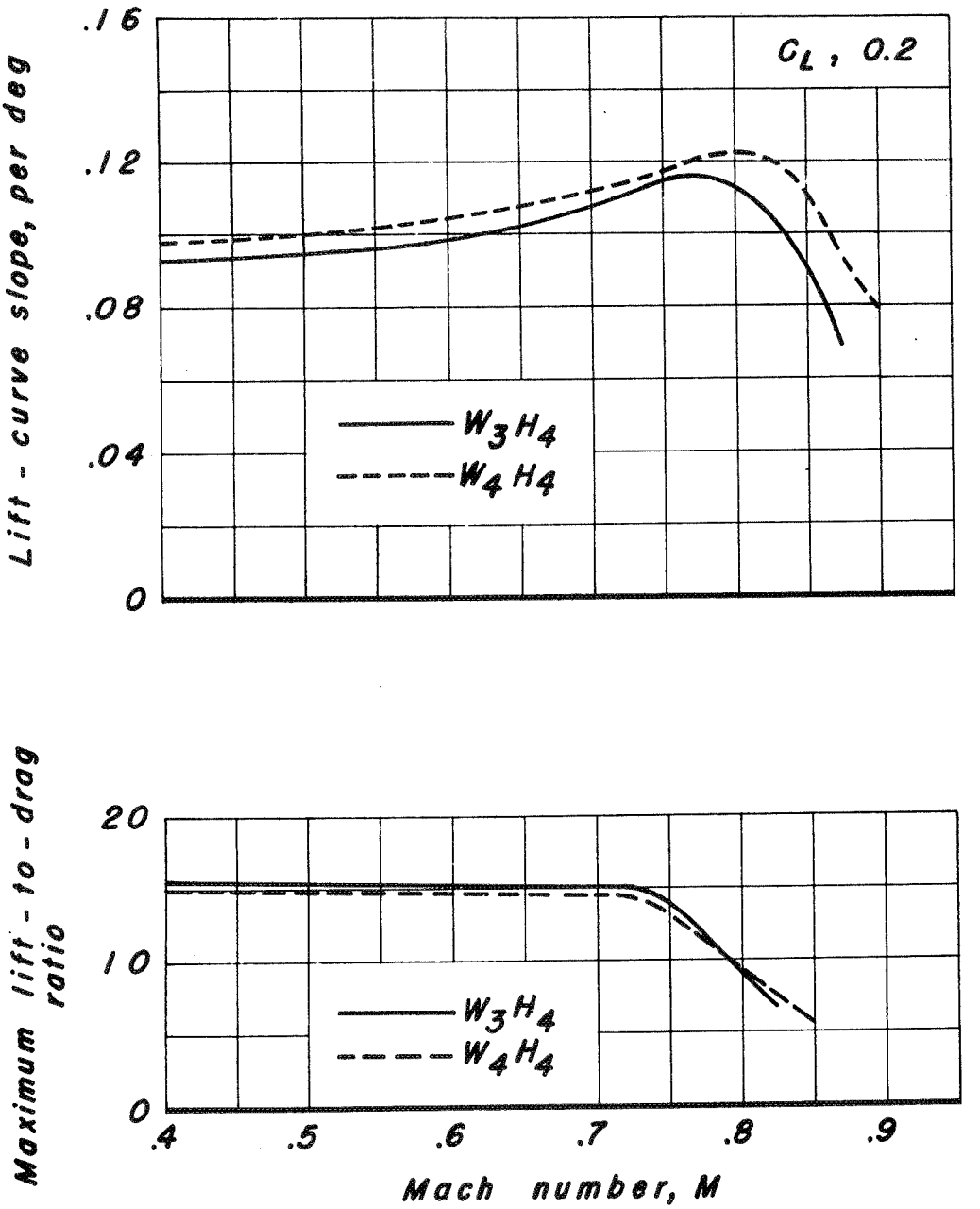

Figure 15.— Variation with Mach number of lift-curve slope and maximum lift-to-drag ratio for W_3H_4 and W_4H_4. δe, 0°.

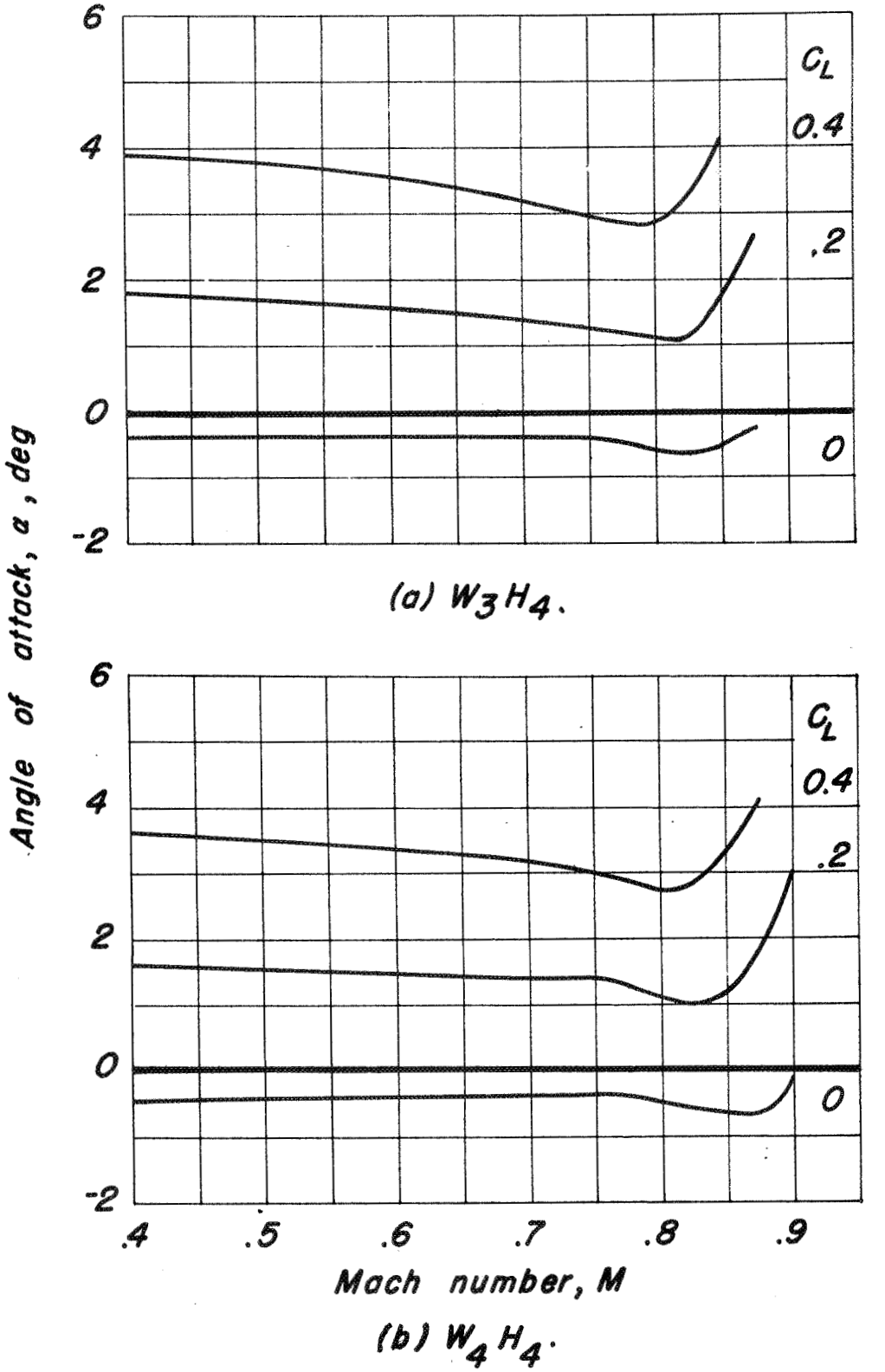

Figure 16.—Variation with Mach number of angle of attack at several lift coefficients for W_3H_4 and W_4H_4.

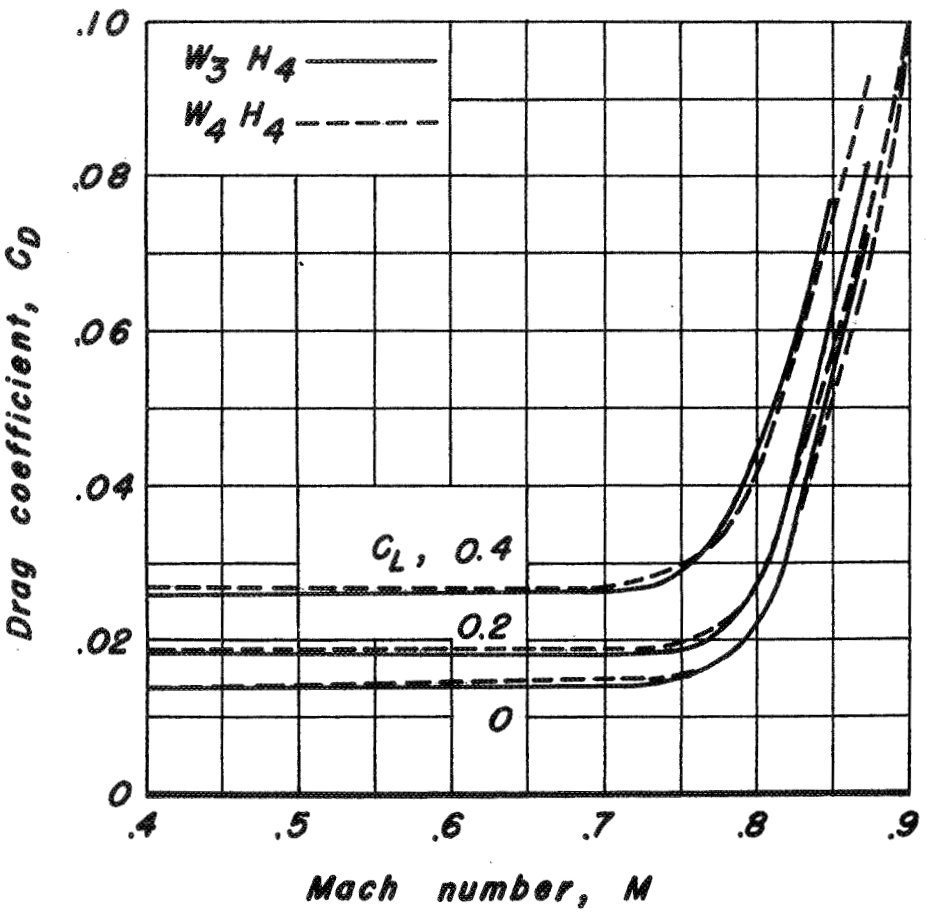

Figure 17.—Variation with Mach number of drag coefficient at several lift coefficients for W_3H_4 and W_4H_4.

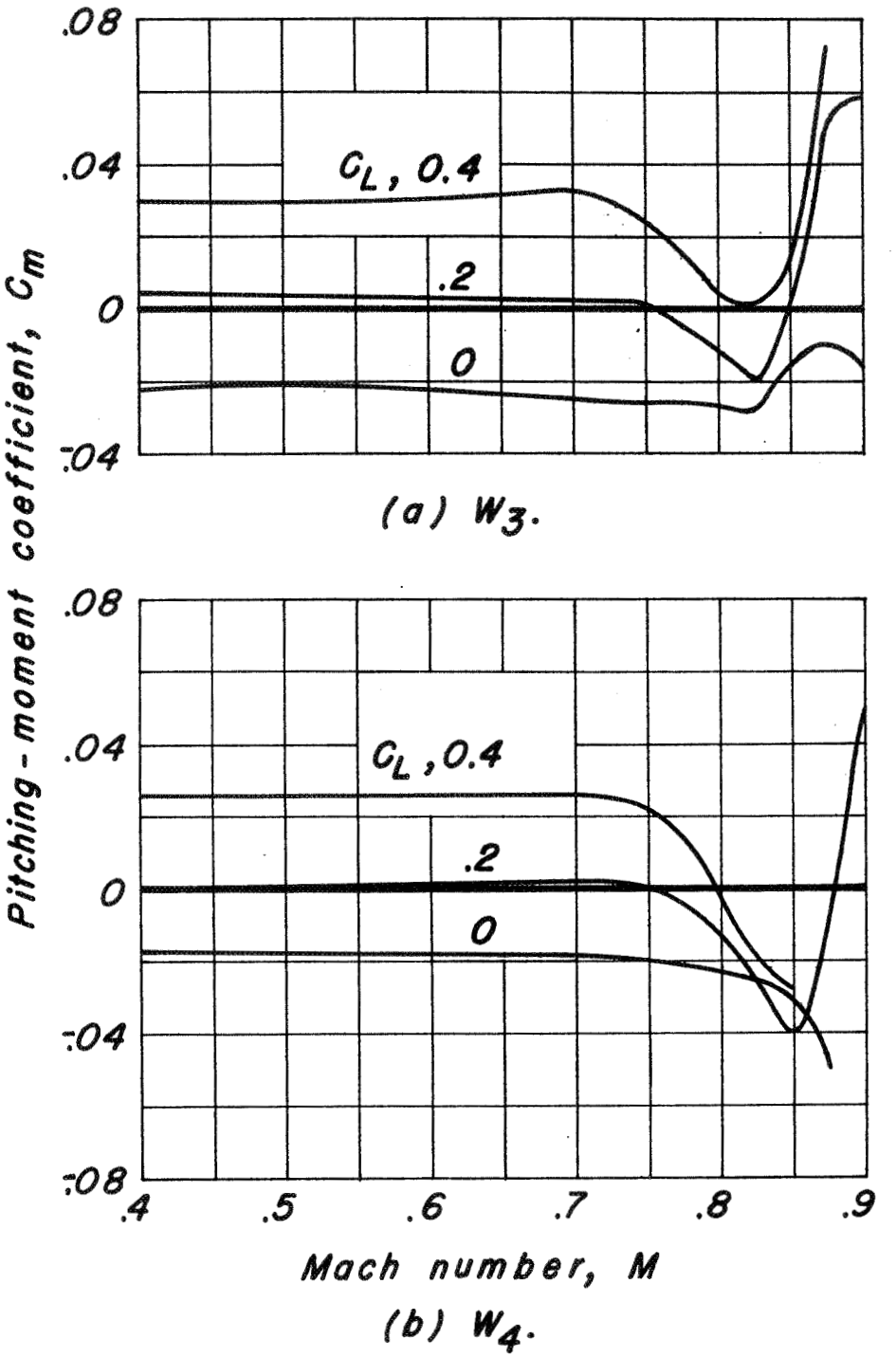

Figure 18.—Variation with Mach number of pitching-moment coefficient at several lift coefficients for the model without tail surfaces.

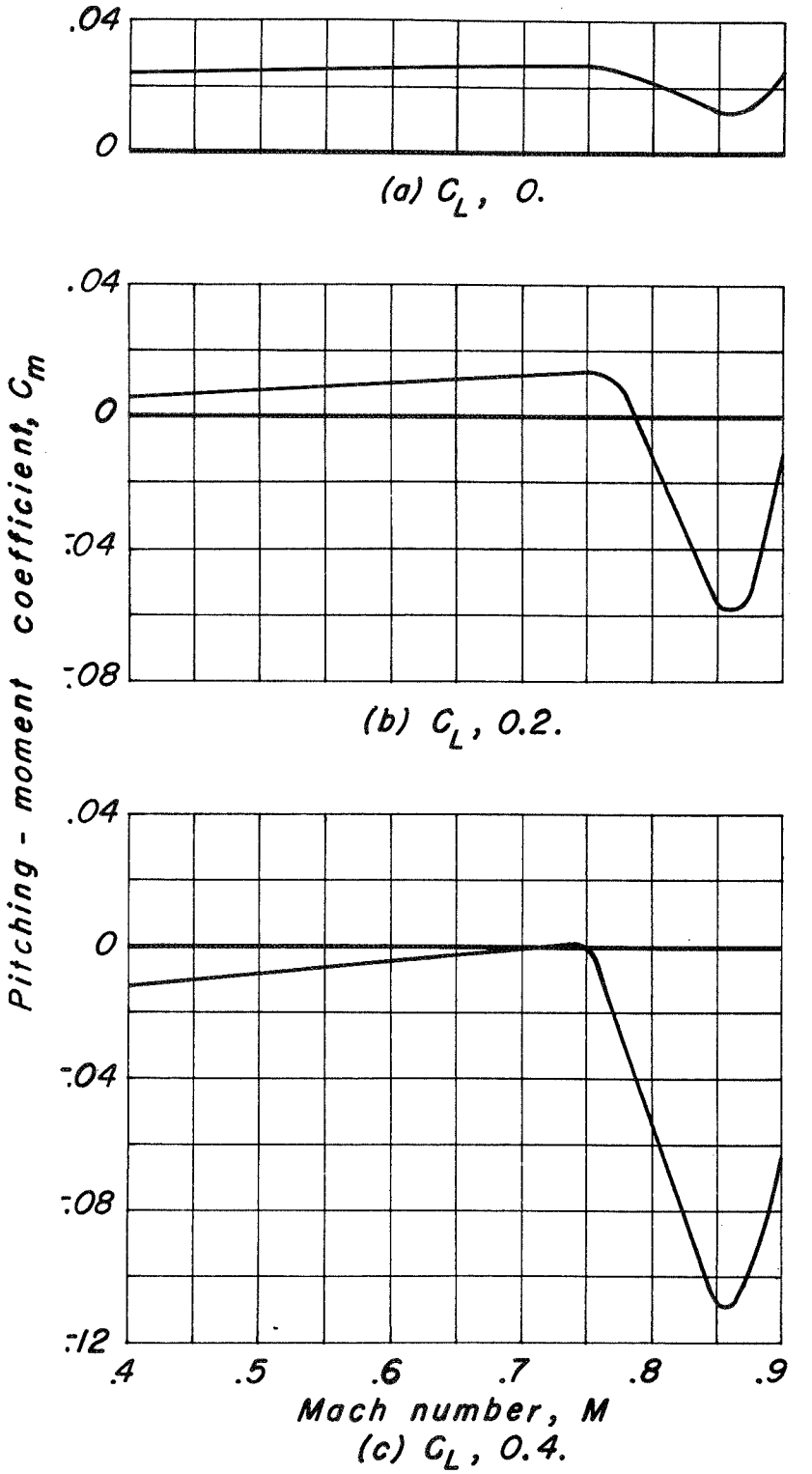

Figure 19.—Variation with Mach number of pitching-moment coefficient at several lift coefficients for W_4H_4. i_t, 0°; δ_e, 0°.

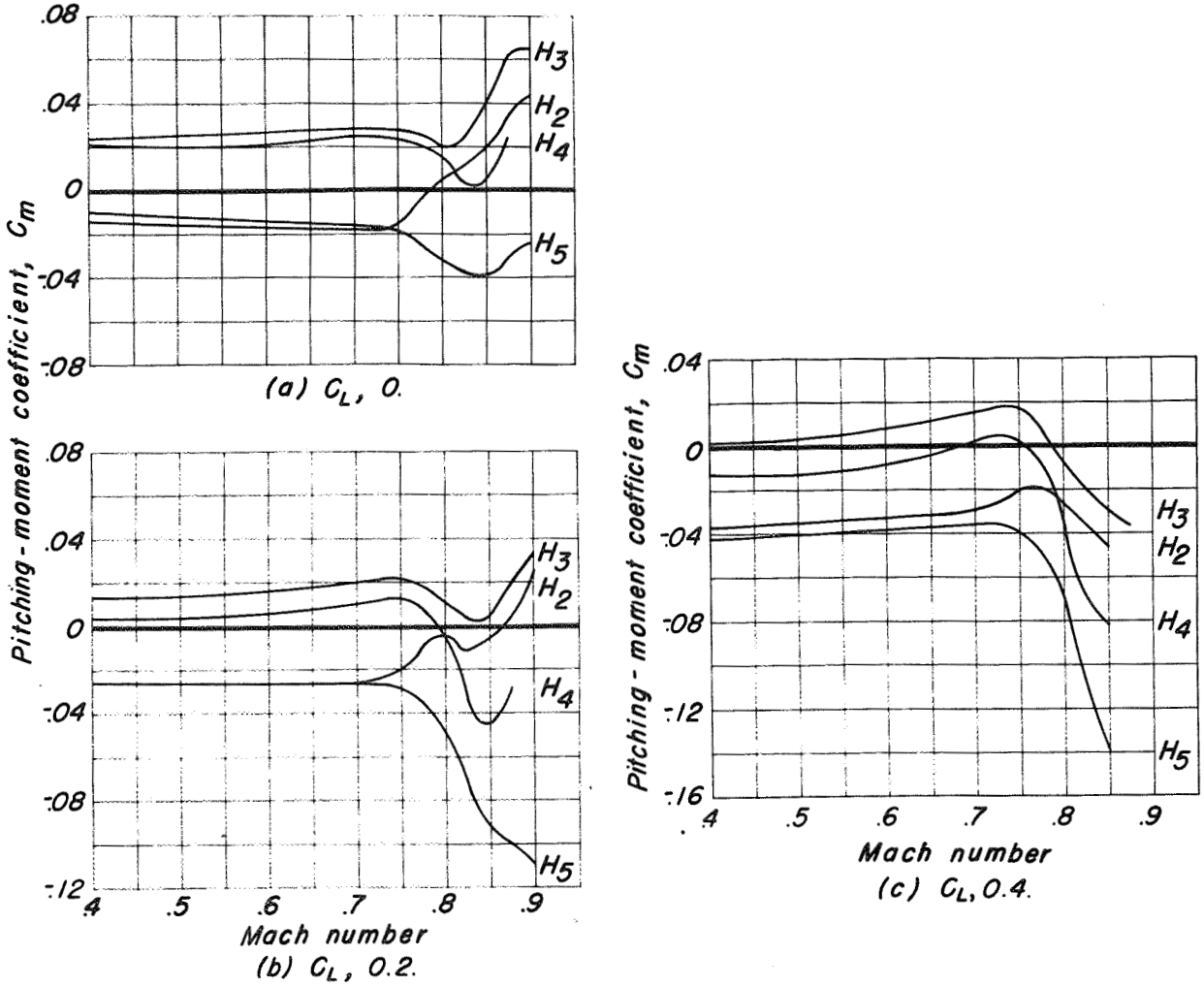

Figure 20.—Variation with Mach number of pitching-moment coefficient at several lift coefficients for W_3 in combination with H_2, H_3, H_4, and H_5. i_t, 0° for H_3, H_4, H_5; i_t, 1° for H_2; δ_e, 0°.

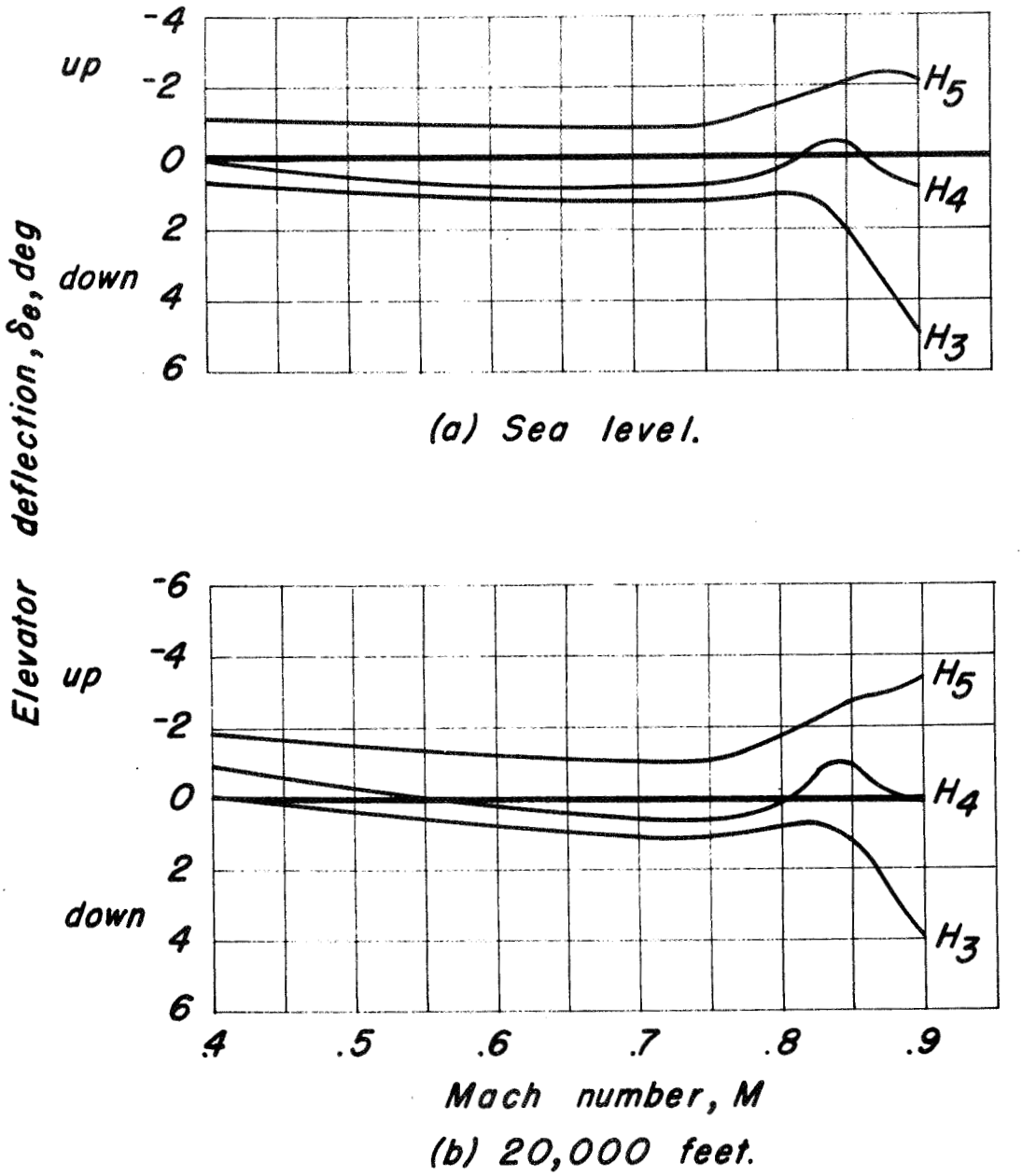

Figure 21.—Estimated elevator deflection required with a wing loading of 50 pounds per square foot for level flight at sea level and at 20,000 feet for W_3H_3, W_3H_4, and W_3W_5. i_t, 0°.

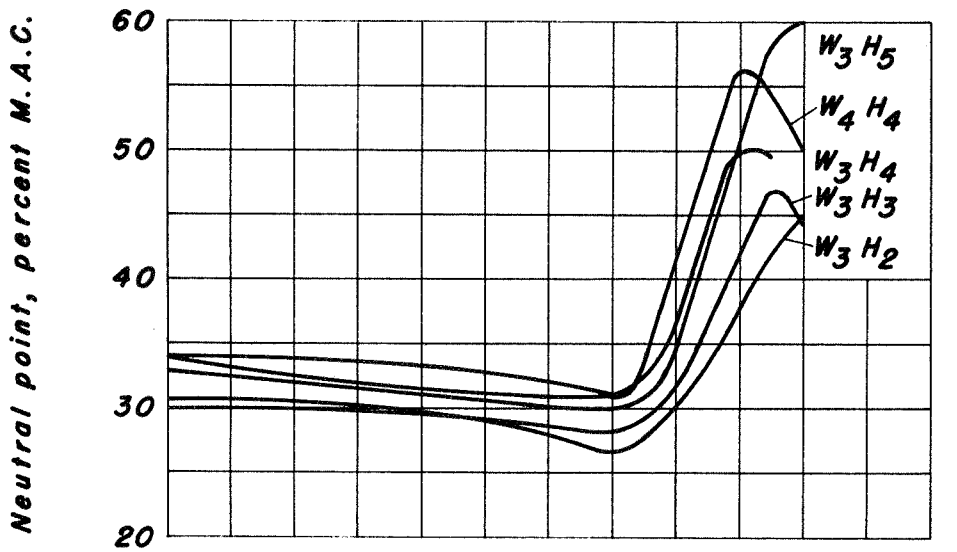

(a) Neutral point, percent M.A.C.

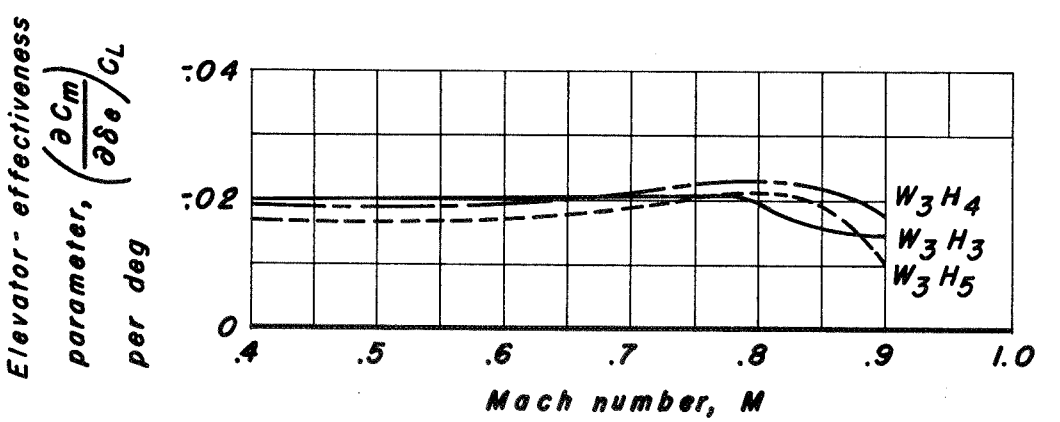

(b) Elevator-effectiveness parameter.

Figure 22.—Variations of the stick-fixed neutral point and of the elevator-effectiveness parameter with Mach number for various wing and tail combinations. C_L, 0.2.

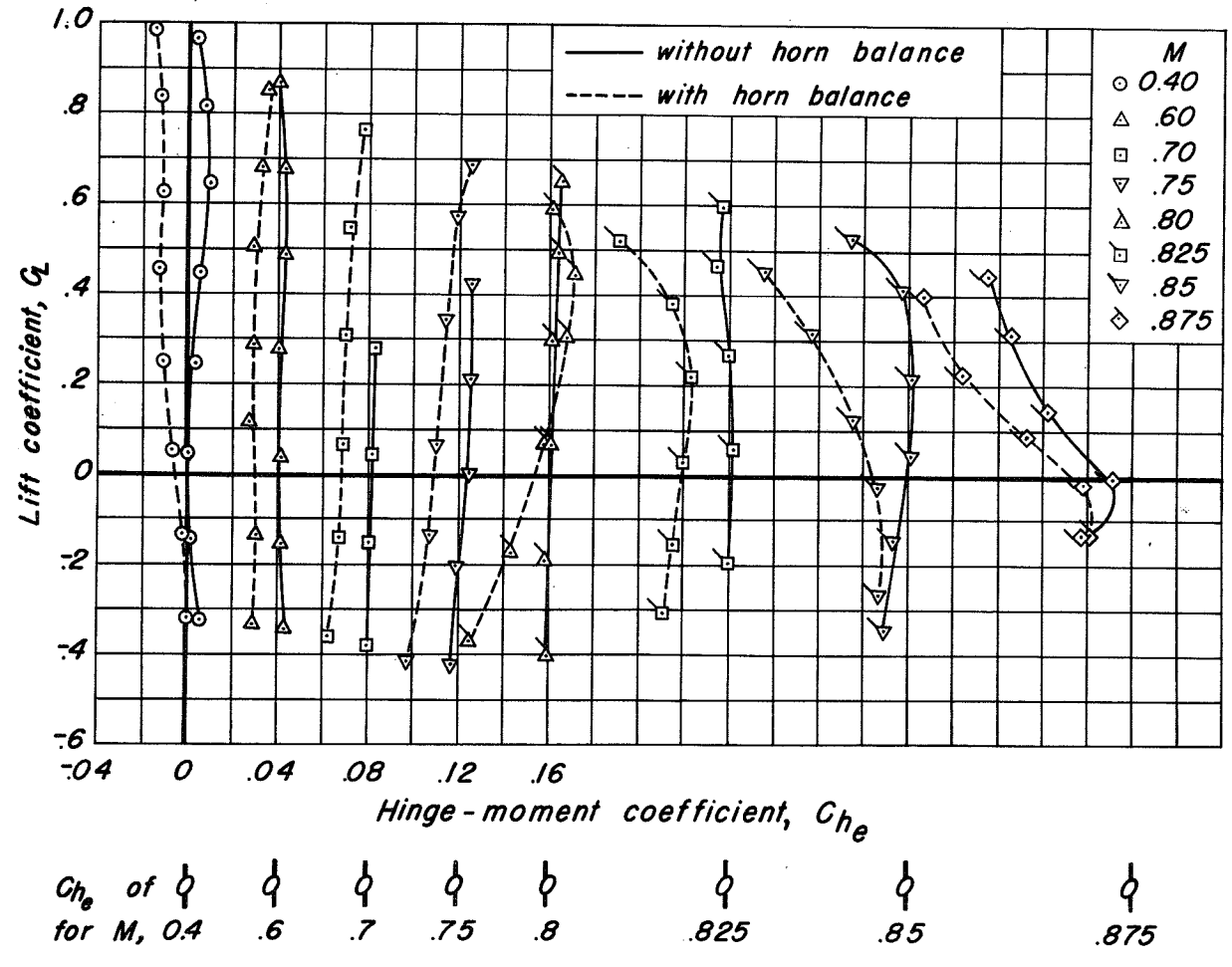

Figure 23.—Variation of elevator hinge-moment coefficient with lift coefficient at various Mach numbers for W_2H_2 with horn balance (data from reference 1) and for W_3H_2 without horn balance. i_t, 1°; δ_e, 0°.

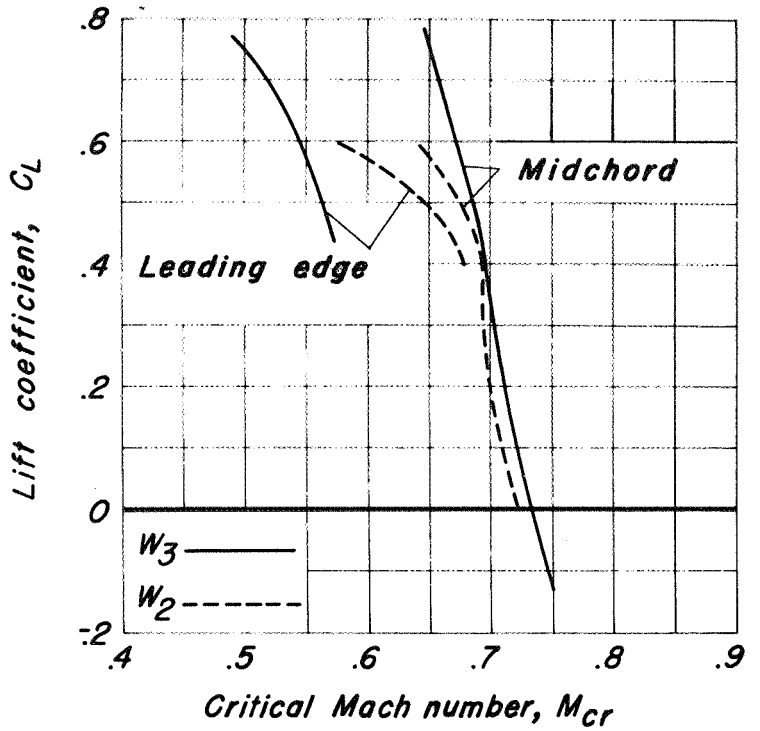

(a) Critical Mach number on upper surface of wing at a lateral distance of 17.41 inches from fuselage center line.

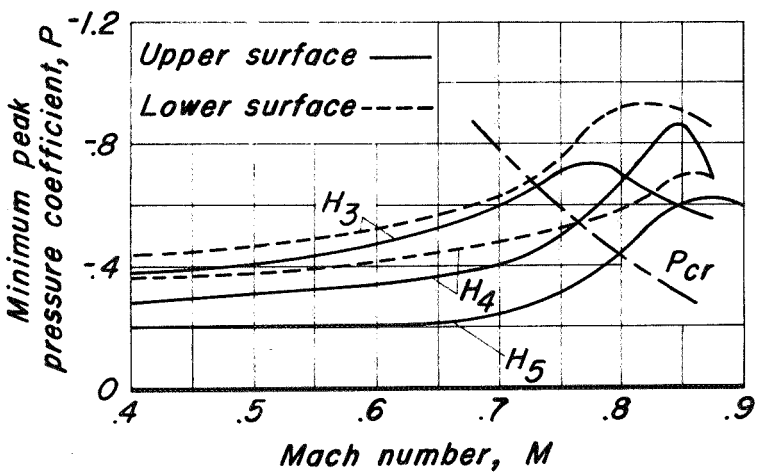

(b) Minimum peak pressure coefficient at tail intersection. Model lift coefficient, 0.2.

Figure 24.— Experimentally determined critical Mach number for the wing and tails.

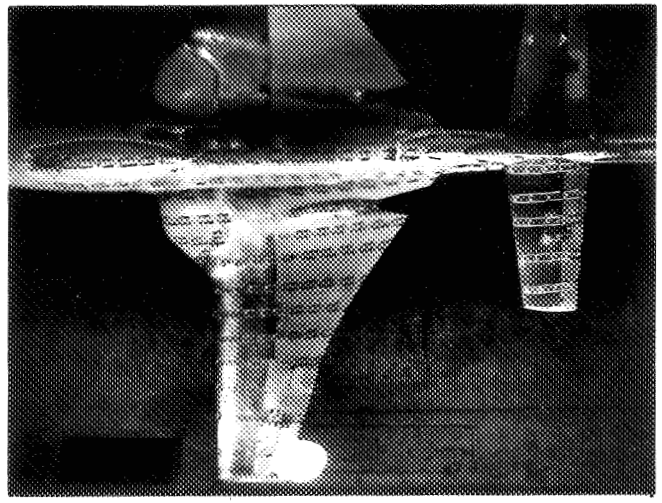

(a) W_3. M,0.775; α_u,2°; C_L,0.36.

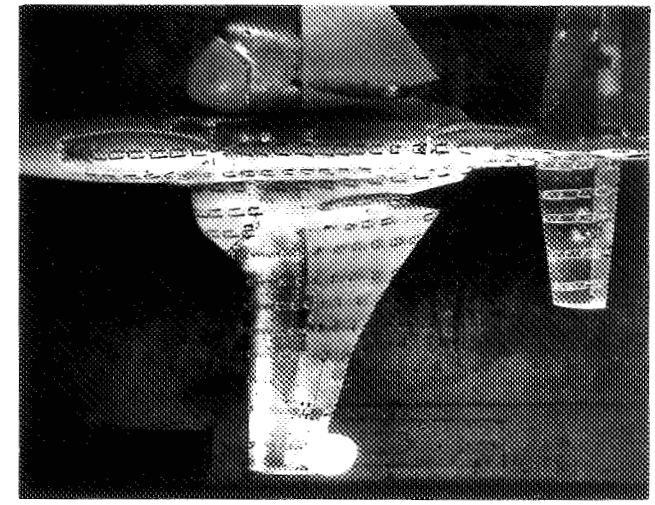

(b) W_3. M,0.825; α_u,0°; C_L,0.10.

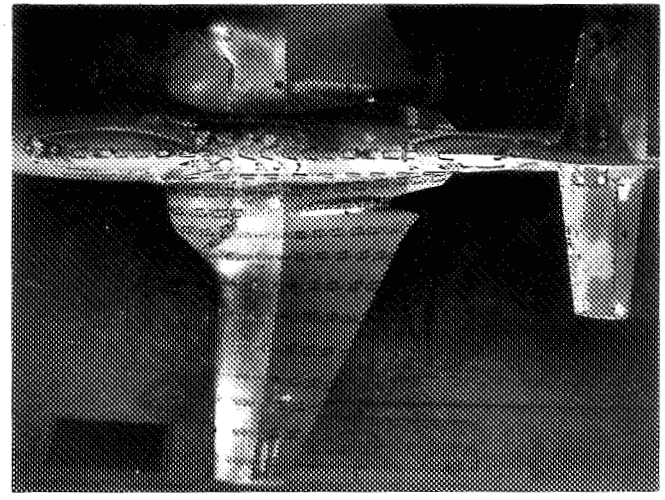

(c) W_4. M,0.775; α_u,2°; C_L,0.30.

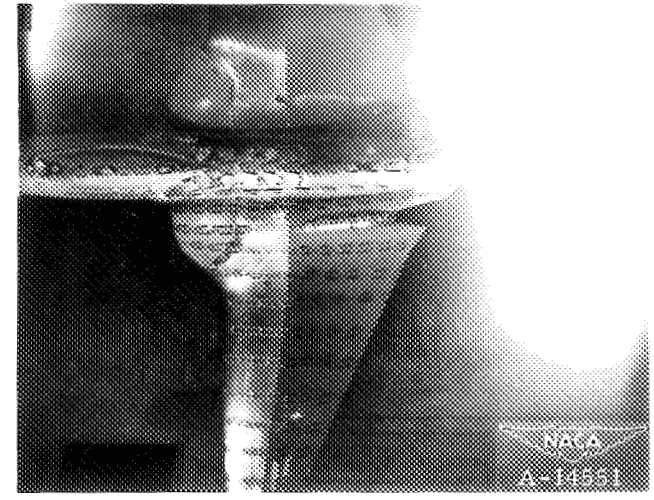

(d) W_4. M,0.825; α_u,0°; C_L,0.08.

Figure 25.- Photograph of tufts on wings W_3 and W_4.

NATIONAL ADVISORY COMMITTEE FOR AERONAUTICS
AMES AERONAUTICAL LABORATORY, MOFFETT FIELD, CALIF.

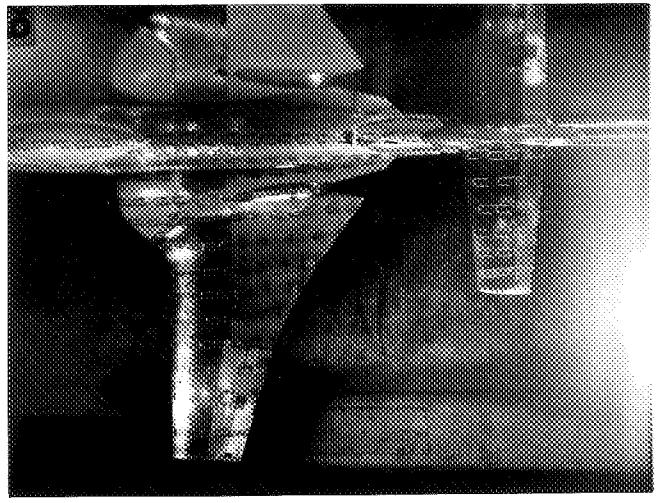

(e) W_3. M,0.85; α_u,2°; C_L,0.22.

(f) W_3. M,0.875; α_u,2°; C_L,0.12.

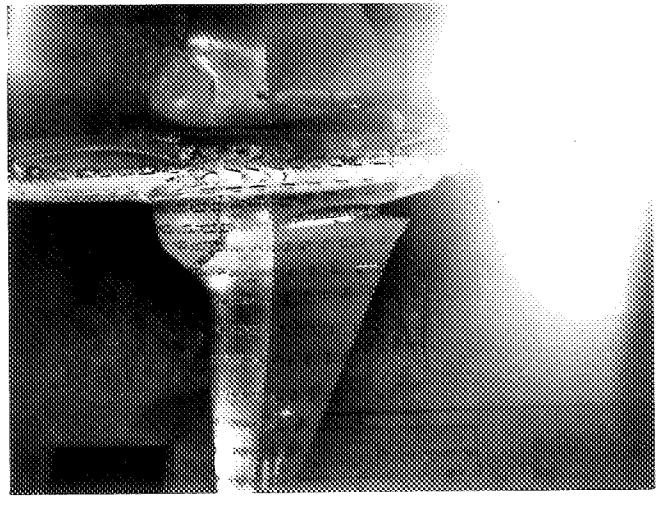

(g) W_4. M,0.85; α_u,2°; C_L,0.29.

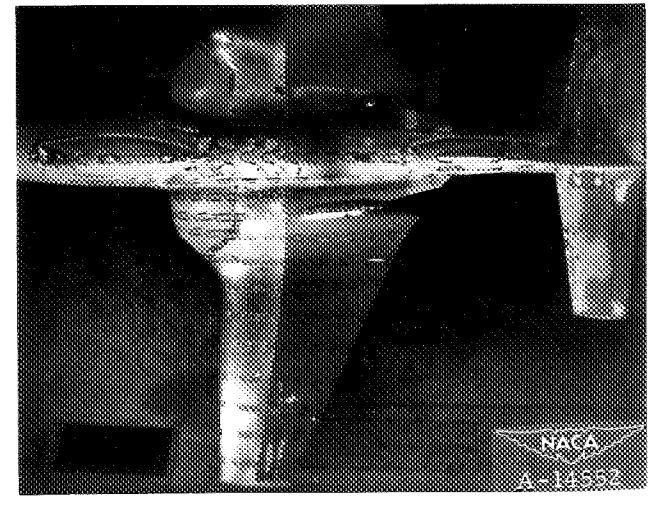

(h) W_4. M,0.875; α_u,2°; C_L,0.23.

Figure 25.- Concluded.

NATIONAL ADVISORY COMMITTEE FOR AERONAUTICS
AMES AERONAUTICAL LABORATORY, MOFFETT FIELD, CALIF.

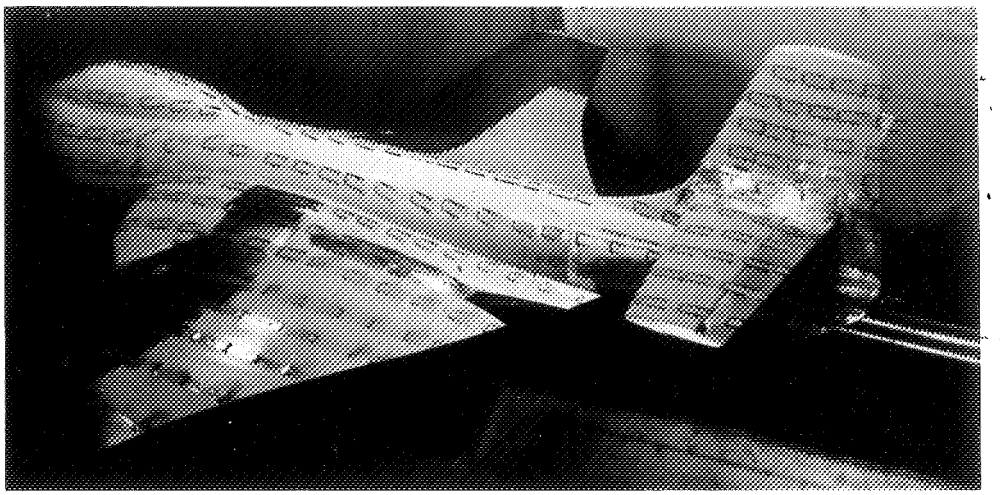

(a) H_3. M,0.85; α_u,2°; C_L,0.17.

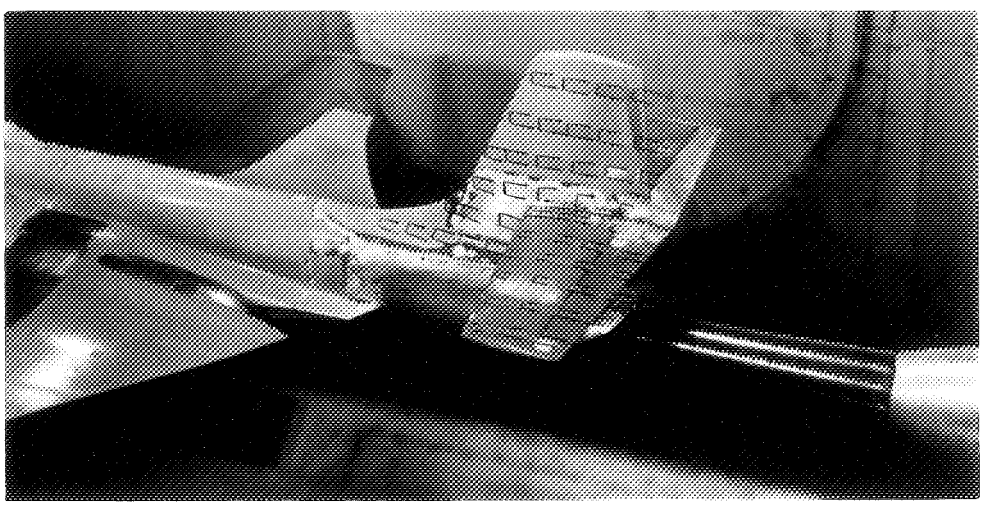

(b) H_4. M,0.85; α_u,2°; C_L,0.24.

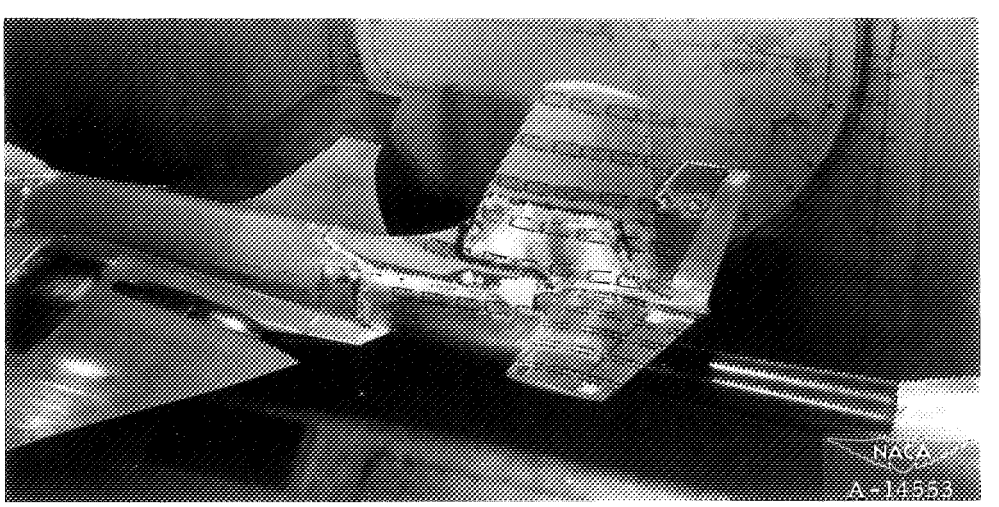

(c) H_5. M,0.85; α_u,2°; C_L,0.25.

Figure 26.— Photographs of tufts on horizontal tails H_3, H_4, and H_5 tested with wing W_3.

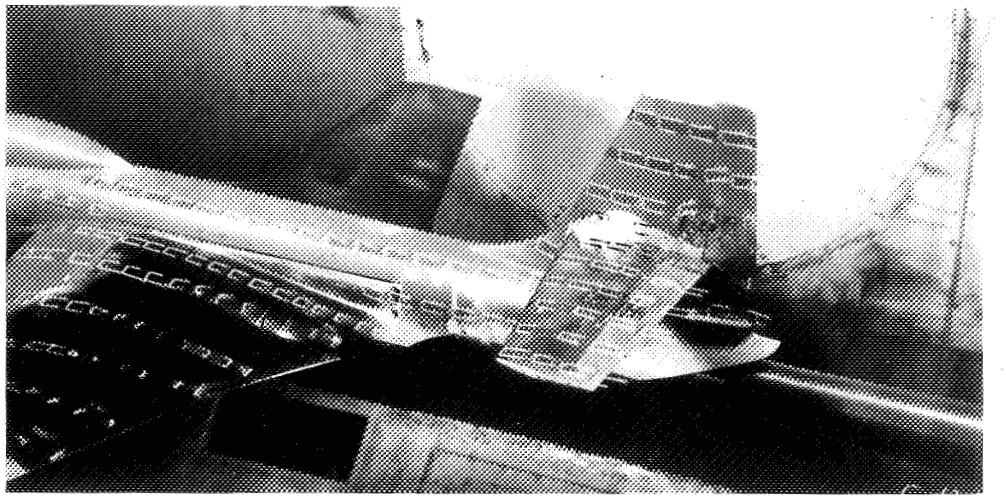

(a) W_2H_2. M,0.85; α_u,2°; C_L,0.12 (from reference 1).

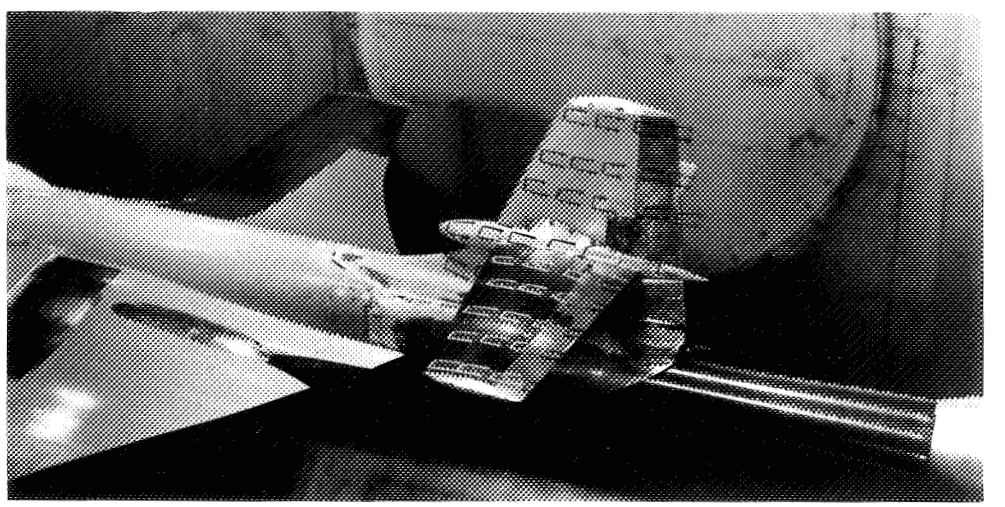

(b) W_3H_2 with bullet fairing. M,0.85; α_u,2°; C_L,0.22.

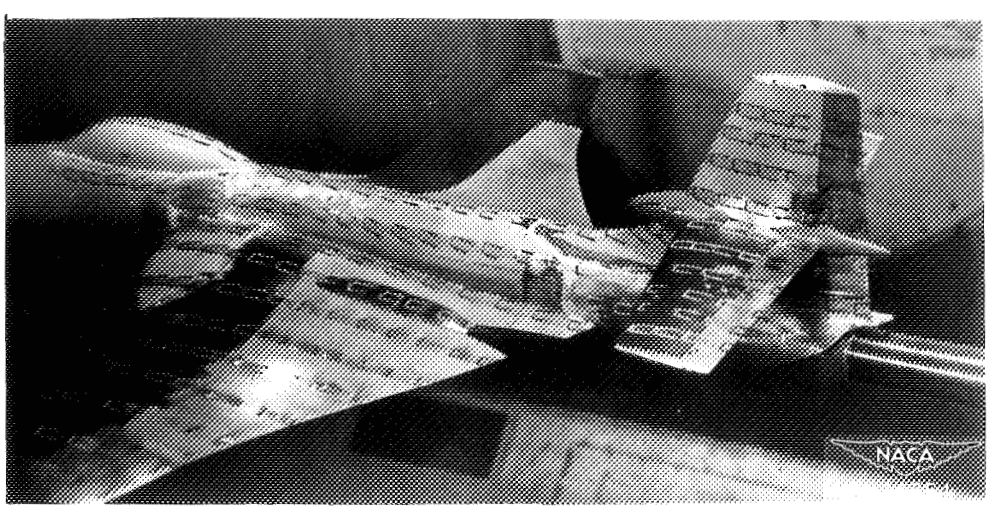

(c) W_3H_2 with hourglass fairing. M,0.85; α_u,2°; C_L,0.22.

Figure 27.– Photographs of tufts on horizontal tail H_2 tested with wings W_2 and W_3.